FINAL SCIENTIFIC/TECHNICAL REPORT

Project Title: Investigation of Coal-biomass Catalytic Gasification using Experiments, Reaction Kinetics and Computational Fluid Dynamics

Type of Report: Final Scientific/Technical

Reporting Period Start Date: October 1, 2010

Reporting Period Start Date: September 30, 2015

Principal Authors: Dr. Francine Battaglia, Dr. Foster Agblevor, Dr. Michael Klein, and Dr. Reza Sheikhi

Date of Report: December 31, 2015

Award Number: DE-FE0005476

Submitting Organization: Virginia Polytechnic Institute and State University
Office of Sponsored Programs
300 Turner Street NW, Suite 4200 (MC 0170)
Blacksburg, Virginia 24061

Subcontractors: Utah State University
Office of Research and Graduate Studies
1415 Old Main Hall
Logan, Utah 84322

University of Delaware
Research Office
210 Hullihen Hall
Newark, Delaware 19716

Northeastern University
Research Administration and Finance
960 Renaissance Park
Boston, Massachusetts 02115

Abstract

A collaborative effort involving experiments, kinetic modeling, and computational fluid dynamics (CFD) was used to understand co-gasification of coal-biomass mixtures. The overall goal of the work was to determine the key reactive properties for coal-biomass mixed fuels. Sub-bituminous coal was mixed with biomass feedstocks to determine the fluidization and gasification characteristics of hybrid poplar wood, switchgrass and corn stover. It was found that corn stover and poplar wood were the best feedstocks to use with coal. The novel approach of this project was the use of a red mud catalyst to improve gasification and lower gasification temperatures. An important results was the reduction of agglomeration of the biomass using the catalyst. An outcome of this work was the characterization of the chemical kinetics and reaction mechanisms of the co-gasification fuels, and the development of a set of models that can be integrated into other modeling environments. The multiphase flow code, MFIX, was used to simulate and predict the hydrodynamics and co-gasification, and results were validated with the experiments. The reaction kinetics modeling was used to develop a smaller set of reactions for tractable CFD calculations that represented the experiments. Finally, an efficient tool was developed, MCHARS, and coupled with MFIX to efficiently simulate the complex reaction kinetics.

Table of Contents

1. Executive Summary

Coal is undoubtedly one of the most important sources of energy, but unfortunately it has a large carbon footprint and other pollution problems associated with it. On the other hand, biomass feedstocks are clean renewable energy sources that can play an important role in the World's energy equation. Since biomass is clean and coal has pollution problems and large carbon footprints, it is conceivable to reduce the negative effects of the coal by combining it with biomass. Current technology of co-combustion of coal and biomass feeds the biomass and coal independently in a combustor and then recombine the product gases for power generation. Most gasification of coal to produce heat and power do not normally include biomass as a feedstock in the process.

Experiments were conducted to assess the co-gasification of coal and biomass. The biomass materials tested included poplar-wood, corn stover and switchgrass. Red mud was also used as a catalyst and its synergistic effect was examined in the co-gasification studies. Gasification was tested at temperatures of 700, 800 and 900 °C and the ratio of coal to biomass material was increased from 0 to 50% (by weight) in increments of 10 wt.%. The major gaseous products from co-gasification experiments were H_2, CO, CO_2, and CH_4. Light molecular weight hydrocarbons (C_2-C_4) were present but at very low concentrations. The co-gasification of poplar wood with coal showed similar trends as the corn stover/coal mixtures except that poplar/coal mixtures did not form any agglomerates when silica sand was used in the fluidized bed reactor. The co-gasification behavior of sub-bituminous coal and hybrid poplar wood mixtures using different media (N_2, CO_2) at low temperatures in a fluidized bed showed additive behavior between coal and poplar co-gasification, which indicated lack of synergetic effects. It appeared the two feedstocks underwent thermal degradation independently, which could be attributed to different temperatures of devolatilization for coal and biomass. In spite of lack of major synergies between coal and poplar, co-gasifying the two feedstocks should be considered a key to a sustainable natural resource management since these mixtures did not form any agglomerates.

The red mud catalyst promoted cracking of char and tars into product gases as their yields were lower compared to those obtained using silica sand. Product gas yields obtained using red mud were slightly higher than product gas yields from silica sand experiments. This could be due to the catalytic effect of red mud compared to silica sand. In the case of the pure coal, the H2/CO ratio decreased with temperature whereas in the case of the coal/corn stover mixture, the ratio remained almost constant. This is a very important finding because it shows how the addition of biomass to coal using red mud as a catalyst can alter the H2/CO ratio and therefore the gaseous products can be tailored to various applications such as Fischer Tropsch liquids or use directly as syngas for combustion. Additionally, the red mud was able to reduce tar formation in the product gas. Also of noteworthy was the absence of agglomeration reaction in the reactor. The alkali metals in the corn stover did not form any agglomerates with the red mud which makes the red mud an ideal gasification medium for coal and biomass mixtures.

The kinetics modeling provided simple lumped models to represent the co-gasification of coal-biomass feeds. It was shown that it is possible to predict the behavior of the biomass fractions; however, further analysis of the biomass and its tar species is needed for future modeling. It was also determined that the condensation of the tar from char is a major source of the solids in the effluent and should not be overlooked in the models. It is possible to model non-oxygen based gasification without considering the diffusion or any type of shrinking core (reactions occur slower as gasification conversion proceeds) or random pore model (reactions occur faster as gasification conversion proceeds). The complexity of a fully molecular model of gasification technology is governed not by the gasification reactions, but by the pyrolysis and the overabundance of tar species.

Attribute reaction modeling may be possible with a much more in depth analysis of the feed solids and the effluent solids and tars. If we put wet coal and gas into the gasifier, there is

enough water produced from drying to drive the steam gasification reactions. It is important to understand the abilities and shortcomings of modeling the kinetics and the computational fluid dynamics so as to produce the proper interface between the two modeling technologies. Future efforts should be able to capitalize on the structure of the tuned models, and with a number of different models available, choose one appropriate for the work at hand. Finally, we have shown the optimal framework for linking kinetic behavior with fluid dynamic design.

A newly designed reaction module to facilitate handing of complex chemical kinetics, MCHARS developed and coupled with the multiphase flow code, MFIX. The interface improved the efficiency of multi-phase reacting flow calculations by splitting the hydrodynamics and chemistry calculation into separate fractional steps. This splitting also improved flexibility and computational efficiency of both solvers. Based on a study of discretization methods, it was found that TVD schemes provided reliable prediction of bubble dynamics and hence, mixing and chemical reaction in the bed. Among the TVD schemes, MC provides favorable prediction of fluidization with relatively less computational cost. Also, the DWF algorithm was computationally advantageous due to its parallel efficiency on distributed memory platforms.

Numerical simulations of fluidized beds were used to better understand the fluidization and particle mixing behavior of coal-biomass mixtures. Also simulations were used to find the best drag model between seven models reported in the literature to simulate coal, poplar wood, and their mixtures. Results of the drag model study revealed that if static regions of material are removed by adjusting the mass in the fluidized bed, the commonly-used drag models for Geldart B particles work well with Geldart A particles. The Gidaspow-blend model proved to be the more reliable drag model for both single solid phases and binary mixtures. The predictions for pressure drop across the bed and bed height were validated with the experiments and found to be in a good agreement. A quantitative analysis of the mixing index confirmed that as the poplar wood mass ratio increased, the quality of mixing improved, with an average mixing index of 62%. Therefore, reasonable amounts of biomass can be added with coal without adverse effects of segregation or elutriation, while reducing the use of a fossil fuel.

The gas-solid reacting flow simulations were carried out using MFIX coupled with the new reaction module. This module provides an efficient and convenient means to implement reactions in MFIX. The gain in computational efficiency is because the reaction module uses a fractional steps method, which separates integration of the chemical reaction into fractional steps. Using this approach the transport equations are advanced with the flow time scale and the integration of chemical reaction is handled using a standard stiff ordinary differential equation solver. The effort included extensive assessment of the module against the results obtained using original MFIX and validations against experimental data. The former shows almost identical comparison between reaction module and original MFIX results. Coal kinetics were implemented in the module and simulations were performed using MFIX-MCHARS. Predictions showed favorable agreement with the experimental data. This study demonstrated the capacity of the reaction module to handle chemical mechanisms as well as its accuracy and efficiency in gas-solid reacting flow simulations. The MCHARS module can be used in the future to consider reaction mechanisms with various levels of complexity in MFIX simulations.

2. Gasification experiments

2.1 Methods

2.1.1 Materials

The following biomass feedstocks were procured from Virginia Tech and Forest Concepts: hybrid poplar wood, switchgrass, and corn stover. The coal samples used for the experiments were obtained from the University of Utah coal combustion laboratory. The coal sample was a sub-bituminous coal obtained from Antelope Coal Mines, WY. The characteristics of the coal are shown in Table 2.1. The coal was pulverized before delivery to the Utah State University Bioenergy Center for use in the gasification studies.

The biomass feedstocks were produced by the Virginia Tech Forestry club and Forest Concepts LLC (Auburn, WA). The logs were first ground using a disc grinder and these were further ground using a Wiley mill (model number 4) at the USTAR Bioenergy Center to pass through a 2-mm mesh screen. The ground biomass and coal samples were characterized for particle size distribution, moisture, and ash contents. Samples of the biomass were also blended with the coal and characterized. The characteristics of the feed biomass, coal, and the blends are shown in Table 2.2.

The particle size distributions of the coal and biomass samples are shown in Fig. 2.1. The particle size distributions of the biomass varied among the three samples despite the fact that they were all ground through the 2-mm mesh screen. These differences in the particle size distribution were attributed to the properties of the individual biomass. The woody biomass was more fibrous and showed a wider particle size distribution. The corn stover and switchgrass, which are both grasses, showed very narrow particle size distribution than the wood. The coal, which is more brittle than the biomass, showed a very wide particle size distribution, but most of the particle sizes were smaller than those of the biomass samples.

Red mud is a waste product from the Bayer process of alumina production from bauxite. The red mud which was supplied by Sherwin Alumina Co LLC, (Gregory, TX), was dried at ambient laboratory conditions, ground with mortar and pestle and sieved to appropriate particle size (125-180 μm) for fluidized bed pyrolysis studies. The composition of the red mud was determined using x-ray diffraction (XRD), and x-ray florescence (XRF) spectrometric analyses, and its surface area was determined using the Quantachrome BET surface analyzer. The x-ray fluorescence (XRF) analysis showed that the red mud was composed of the following major metal oxides (wt. %): Fe_2O_3 (53.98), Al_2O_3 (13.53), SiO_2 (8.91), CaO (8.87), TiO_2 (6.18), and Na_2O (5.83). The presence of these oxides was further confirmed with x-ray diffraction (XRD) analysis. The BET surface area was 30 m^2/g.

Table 2.1 Composition of North Antelope sub-bituminous coal used for the studies

Sample	Composition (%)
North Antelope PRB	
Loss on drying (LOD)	23.69
Ash at 750^{o}C (%)	4.94
C (%)	53.72
H (%)	6.22
N (%)	0.78
S (%)	0.23
O by difference (%)	34.11
Volatile matter (%)	33.36
Fixed carbon (%)	38.01
HHV (MJ/kg)	21.06

Table 2.2 Moisture and ash contents of coal, biomass, and coal/biomass blend samples

Samples	Moisture (wt.%)	Ash (wt.%)
Poplar	5.22±0.29	0.62±0.09
Switchgrass	6.30±0.13	6.17±0.22
Corn stover	6.12±0.43	13.05±0.28
Coal	22.58±0.49	4.94
Poplar: Coal = 70: 30	8.76±0.43	2.07±0.28
Switchgrass: Coal = 70: 30	9.50±1.39	5.74±0.17
Corn stover: Coal = 70: 30	7.86±0.52	8.21±0.09
Poplar: Coal = 50: 50	11.45±0.48	3.22±0.32
Switchgrass: Coal = 50: 50	11.97±0.75	6.62±0.23
Corn stover: Coal = 50: 50	13.36±2.52	11.93±2.68
Poplar: Coal = 30: 70	15.56±1.07	4.30±0.35
Switchgrass: Coal = 30: 70	13.86±1.39	6.79±0.5
Corn stover: Coal = 30: 70	15.14±0.77	8.85±1.13

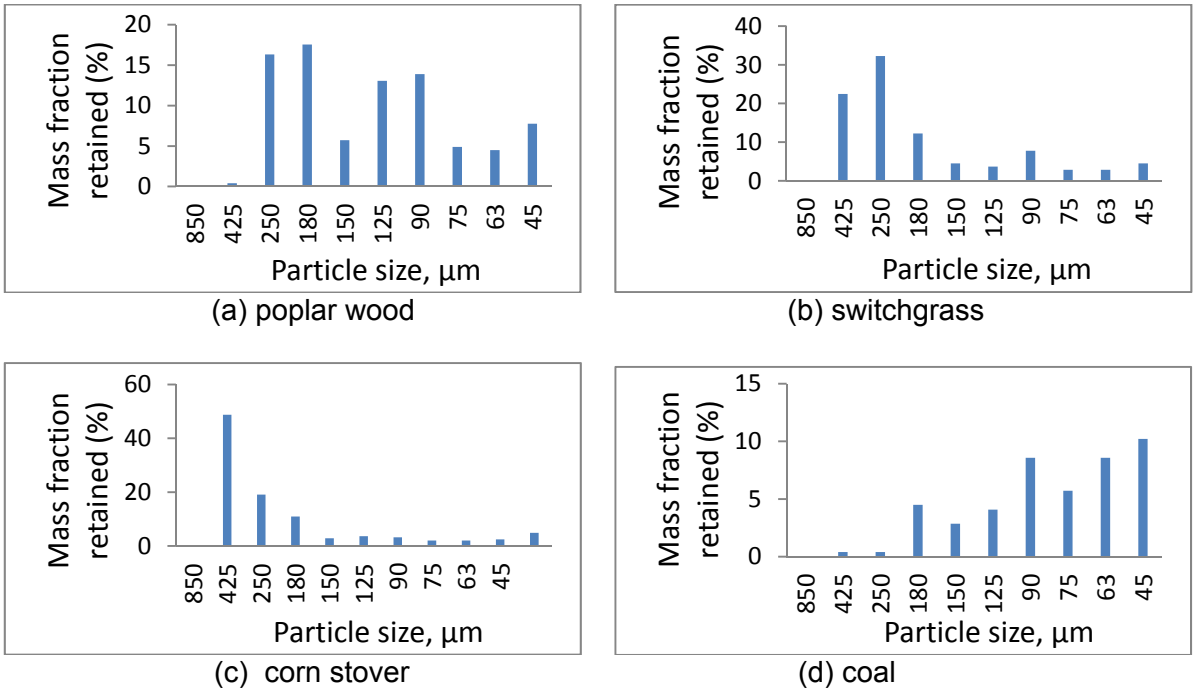

Figure 2.1. Particle size distribution of (a-c) ground biomass and (d) pulverized Antelope sub-bituminous coal

2.1.2 Experimental methods

Samples of the biomass feedstocks, coal and blends were analyzed using TA Instruments thermogrametric analyzer (Q500, TA Instruments, Lindon UT). Analyses were carried from room temperature to 900 ^{o} C at a heating rate of 10 ^{o}C/min. Coal, biomass, and biomass/coal blends were fluidized in a glass fluidized bed reactor in order to provide data for both modeling and information on how the samples will behave in the hot fluidized bed reactor. Pressure drops across the beds, bed heights, and gas flow rates were measured. Nitrogen was used as the fluidization gas.

Biomass, coal and biomass/coal blends were gasified in a two-inch fluidized bed reactor whose schematic diagram is shown in Fig. 2.2. The gasification was carried out at 700, 800, and 900 ^{o}C for all samples and the experiments were conducted in triplicates. The feed was fed into a hopper and nitrogen or suitable gas was used to entrain the feed and conveyed through air cooled jacketed feed tube into the reaction zone. The fluidizing gas was fed from the bottom of the reactor and the fluidizing medium was 100 g of silica sand. The products were passed through a hot gas filter, two ethylene-glycol-cooled condensers, an electrostatic precipitator and finally through coalescing filter and gas totalizer. A slip stream of the gaseous products was connected to a 490 microGC (Agilent Technologies, Santa Clara, CA) for online gas analysis. The excess gas was vented into a fumehood. The reactor, condensers, and hot gas filter were weighed before and after each experiment to determine the gravimetric yields of liquid, solid, and gas products. Gas yield was also determined from the chromatographic analysis and compared with gas yields determined by difference. The gasification was conducted using nitrogen and carbon dioxide as the fluidizing medium.

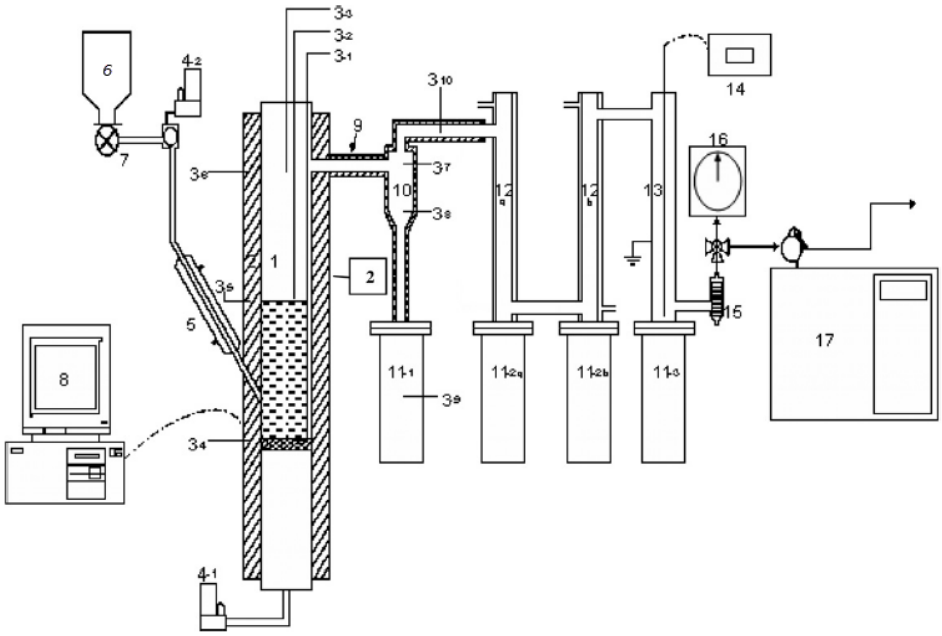

Figure 2.2. Experimental setup of fluidized bed reactor unit (1-fluidized bed, 2-furnance, 3-thermocouple, 4-mass flow controller, 5-jacketed air-cooled feeder tube, 6-hopper, 7- screw feeder, 8-computer, 9-heating tape, 10-hot gas filter, 11-reservoir, 12-condenser, 13-ESP, 14-AC power supply, 15-filter, 16-wet gas meter, 17-gas chromatography)

The gasification reactions described above were also conducted on the same feedstocks using red mud as the gasification medium instead of silica sand. Thus, about 120 g of red mud was loaded into the fluidized reactor and fluidized using nitrogen gas. The coal and other feedstocks were fed into the bed and gasified at 700, 800, and 900 ^{o}C. Product collection and characterization were similar to those carried out for the gasification using the silica sand pyrolysis medium.

2.2 Results

2.2.1 Thermogravimetric analysis of coal and coal/biomass mixtures

The thermogravimetric analysis (TGA) analysis of the coal, biomass, and coal/biomass blends showed two major weight loss regimes for all the blends of coal/biomass. The first minor peak was due to water loss associated with the biomass and coal and this occurred after 100^{o}C. The first major peak had a shoulder and this was attributed to the decomposition of the biomass at maximum temperature of 350^{o}C. The next major peak was attributed to the decomposition of volatiles in coal and had a maximum at 452^{o}C. Poplar had a maximum weight loss at 350^{o}C and coal had its maximum weight loss at 425^{o}C. However, as the percentage of biomass decreased in the blend, the thermal conversion also decreased. This trend was the opposite in coal- as the percentage of coal increased in the blend, its thermal conversion increases. No peak shift was observed with the different blend ratios. The overlap of the peaks of coal and biomass peaks suggests that there could be interaction between the decomposition products from the two feedstocks. However, as will be shown with fluidized bed gasification, although the degradation products mixed, there appeared to be very little synergistic effect. Thus, in practice they appeared to behaving independent of each other.

2.2.2 Fluidization characteristics of coal, biomass and coal/biomass mixtures

The physical properties of the coal and biomass particles are shown in Table 2.3. In general the biomass particles were larger than the coal particles because of the fibrous nature of the biomass. The coal is brittle and was much easier to grind and produced much smaller particles than the biomass. The fluidization pattern of the coal, biomass and various mixtures are shown in Fig. 2.3-2.5. The biomass materials in general had channeling problems as shown in Fig. 2.4 and they tended to bridge in the cold fluidization vessel, however, it is expected that in the hot reactor, because there will be decrease in particle size due to devolitization, this may influence the fluidization pattern and overcome the bridging problem observed in the cold state.

Table 2.3. Physical properties of test materials.

Material	Mean diameter, d_m *(μm)*	Bulk density, ρ_b *(g/cm^3)*	Particle density, ρ_s (g/cm^3)	Estimated sphericity, ψ	Porosity, *Φ*	Geldart classification
Hybrid poplar	152.65 ± 1.21	0.16 ± 0.02	0.35 ± 0.05	0.59 ± 0.05	0.86	A
Switchgrass	144.77 ± 0.70	0.19 ± 0.01	0.32 ± 0.04	0.65 ± 0.04	0.83	A
Corn stover	417.77 ± 1.64	0.21 ± 0.01	0.37 ± 0.01	0.62 ± 0.05	0.83	B
Coal	61.62 ± 0.51	0.49 ± 0.01	1.38 ± 0.01	0.95 ± 0.02	0.64	A
Sand	251.39 ± 0.17	1.51 ± 0.04	2.62 ± 0.01	0.93 ± 0.01	0.42	B

Pressure fluctuations in fluidized-bed systems play important role in understanding the flow behavior and hydrodynamics of particles [1]. In this study, fluidization was described using pressure drop ΔP measured across bed materials and corresponding gas velocities. From Fig. 2.3a-d, it can be seen that coal and biomass particles exhibited a hysteresis effect, which occurs when pressure drop or bed height during fluidization and defluidization gives a different path or are dependent on gas velocity [2]. The hysteresis effect in fluidized beds can be due to: a) interparticle cohesive forces, b) particle-sidewall friction, and c) small fluidized-bed diameter ([3-7]. These factors cause pressure overshoot resulting from yield stress generated between inter-particle and particle-wall interactions during fluidization [6]. Pressure overshoot was observed in pulverized coal (Fig. 2.3a), poplar (Fig. 2.3b), and corn stover (Fig. 2.3c) bed materials. Generally, pressure overshoot and hysteresis effect are typical of Geldart A particles [6, 7]. No pressure overshoot was observed with switchgrass (Fig. 2.3d) because the particle size for these samples fell with the Geldart B classification. However corn stover was also classified as Geldart B particle exhibited hysteresis, which suggested that particle size alone cannot account for the hysteresis effect in biomass particles. Kwauk (1998) suggested that hysteresis can be caused by particle transport i.e., elutriation in dense phase and jetting in dilute phase of fluidized-bed material. Because of the irregular particle sizes of biomass used, fine particle entrainment was observed which led to about 2 g (6.7 %) of fines transported into cyclone dust collector. For the biomass materials, Fig. 2.3b-d show typical features of solid particle entrainment at phase D-E; for the coal, it occurred at phase C-D in Fig. 2.3a. Within the interval of complete fluidization, the pressure drops for the single test materials follow in an increasing order: hybrid poplar (65 Pa) < sub-bituminous coal (72 Pa) < switchgrass (82 Pa) < corn stover (118 Pa).

Fluidization characteristics presented in Fig. 2.5a (coal-poplar), Fig. 2.5b (coal-corn stover), and Fig. 2.5c (coal-switchgrass) show distinct fluidization behavior for binary bed materials compared to those of single bed materials. For some coal-biomass mixtures, the ΔP for mixtures was higher than those of single coal and biomass at complete fluidization phase. The higher pressure drop was attributed to the irregular shape of the biomass particles which could easily cause bridging and trap fine coal particles. The entrapment of smaller particle in the mesh causes the bed mass to become heavier requiring a high pressure to break the mesh for full fluidization to occur, and particle interlocking has been reported [8, 9].

Figure 2.5c shows a completely different trend for 30%, 40%, and 50% switchgrass composition. Their fluidization curves changed significantly with increasing superficial velocity, however ΔP for 40% composition reached a maximum value of 130 Pa at 0.08 m/s superficial velocity before stabilizing. In the case of coal-corn stover fluidization (Fig. 2.5b), ΔP for 30% and 40% corn stover composition were constant at 128 Pa whereas ΔP for 10%, 20% and 50% mixtures were similar to corn stover alone.

The influence of biomass ratios on U_{mf} values suggests that coal-biomass mixtures are likely to vary depending on biomass type and composition. No specific trend was observed with an increase in biomass ratio. With the exception of coal-corn stover mixtures (Fig. 2.5b), the transition behavior of the binary bed materials for coal-poplar (Fig. 2.5a) and coal-switchgrass (Fig. 2.5c) varied greatly from fixed-bed phase to complete fluidization phase. The lack of trend in U_{mf} data for these binary materials could be due to the concentration and distribution of solid particles in the packed bed [10]. In all cases of the coal-biomass study, as the gas flow rate was increased from zero, the binary bed material tend to mix partially however the occurrence of incomplete mixing diminished at complete fluidization. The pressure drops of coal-biomass mixtures were higher than those for single coal and biomass bed materials in the complete fluidization regime. For 40 wt.% and 50 wt.% hybrid poplar and switchgrass content in coal, the bed materials tend to channel up to a certain gas velocity. The development of channeling in the bed materials created difficulties during material fluidization (Fig. 2.4).

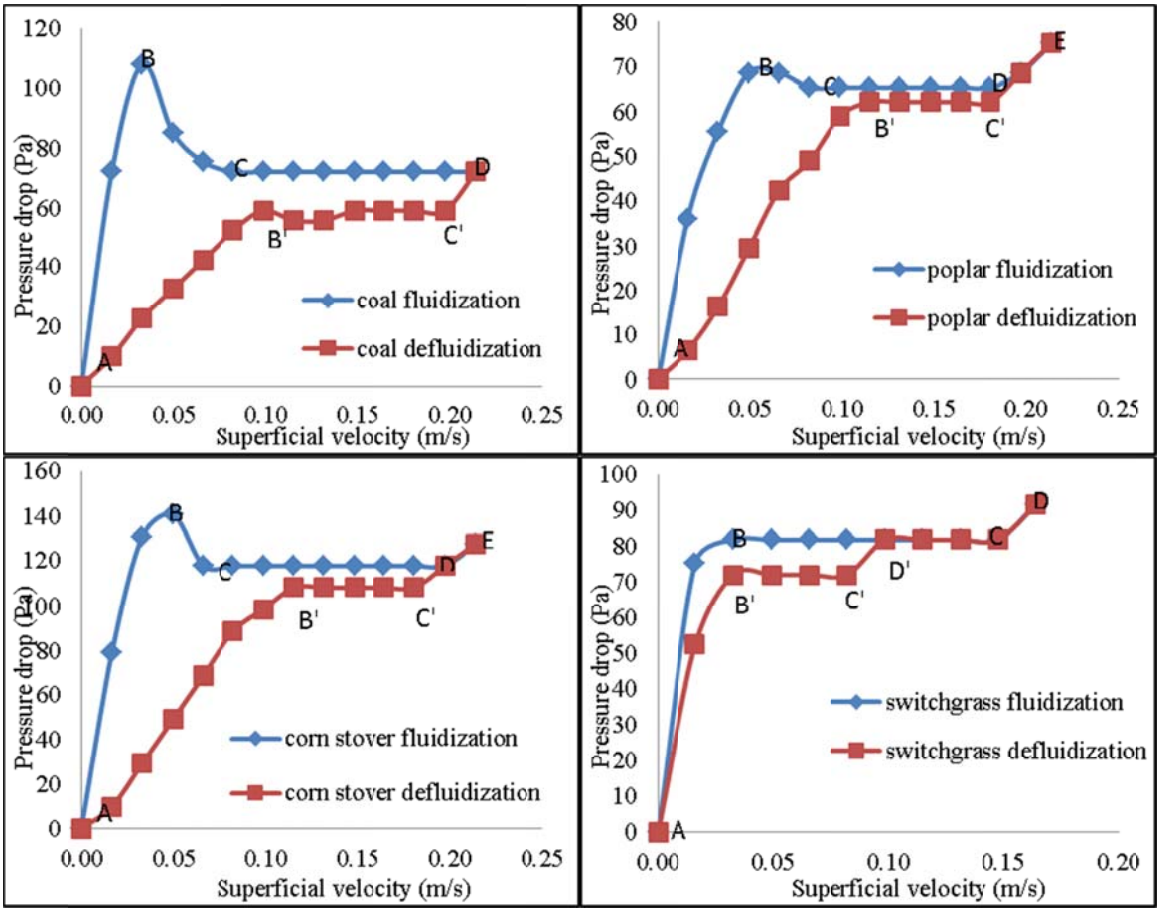

Figure 2.3. Fluidization and defluidization patterns of coal and biomass feedstocks: a) coal; b) poplar wood; (c) corn stover; and d) switchgrass.

Figure 2.4. Channeling observed in the cold fluidization units of biomass and coal/biomass mixtures.

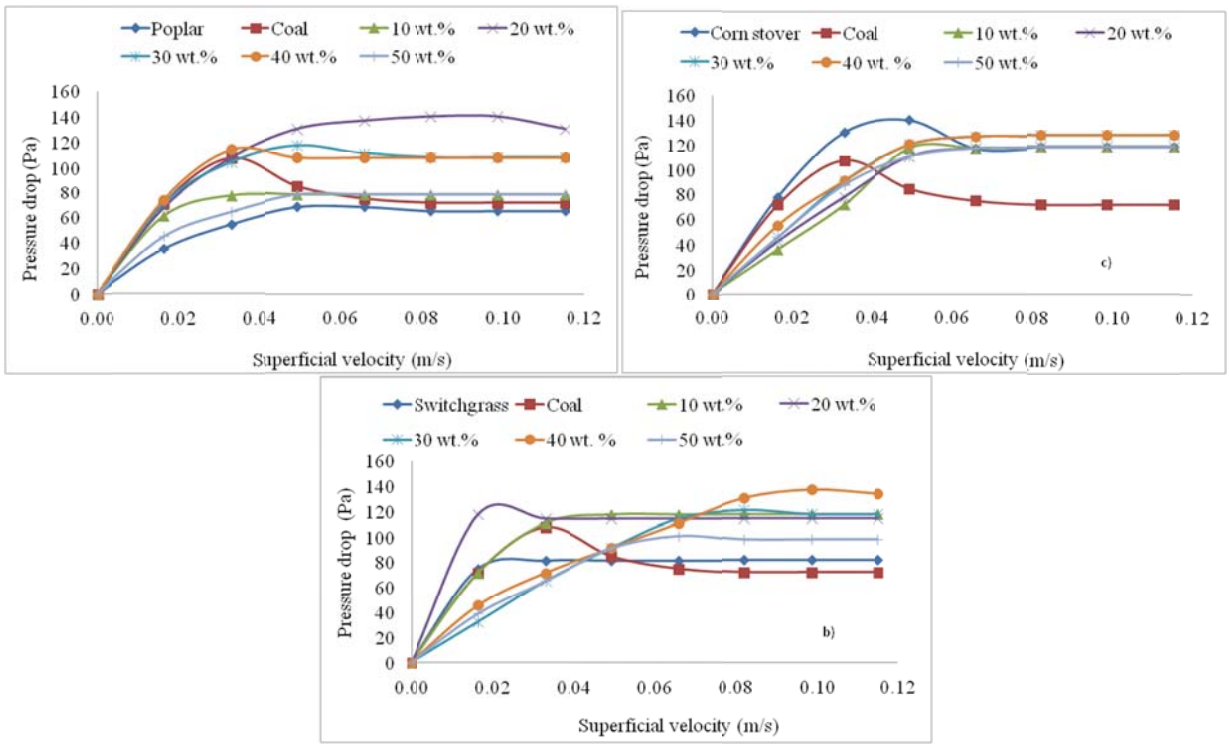

Figure 2.5. Cold fluidization of binary mixtures of coal and various biomass feedstocks: a) coal/polar mixture; b) coal/corn stover mixture; c) coal/switchgrass mixture.

2.2.3 Gasification of coal and coal/biomass mixtures on sand

The coal and biomass feedstocks gasification were conducted for individual feedstocks and binary mixtures. The coal was gasified as received without drying.

Corn stover and coal gasification

The product yields obtained from corn stover gasification in N_2 and CO_2 medium are shown in Table 2.5. Char yields obtained using CO_2 medium were twice as high as char yields from N_2 medium. In contrast, tar yields in CO_2 medium were lower than in N_2 medium. In general, char and tar yields decreased with increasing temperature with corresponding increase in product gas yields. Corn stover product gas yield in nitrogen medium increased from 51 wt.% (all product yields are dry wt.%) at 700°C to 82 wt.% at 900°C and in CO_2 medium, gas yield increased from 48 wt.% at 700°C to 63 wt.% at 900°C.

Table 2.5. Product yield (dry wt.%) for corn stover gasification.

Gasification medium	Temperature (°C)	Char	Water	Tar	Gas
Nitrogen	700	11.37 ±1.21	19.01 ±0.92	16.77 ±1.01	50.84 ±1.65
	800	6.80 ±0.97	20.22 ±1.05	5.44 ±0.89	66.00 ±1.02
	900	4.49 ±1.12	10.65 ±0.76	1.70 ±0.11	81.99 ±0.99
Carbon dioxide	700	18.20 ±1.34	25.32 ±0.56	6.48 ±1.13	48.35 ±0.65
	800	12.37 ±1.65	24.02 ±1.19	4.08 ±0.28	57.91 ±1.09
	900	9.83 ±0.52	25.08 ±0.62	1.00 ±0.31	63.37 ±1.75

Table 2.6. Product yield (dry wt.%) for sub-bituminous coal and corn stover mixtures co-gasification in N_2 medium.

Biomass content (wt.%)	Temp. (°C)	Char		Water		Tar		Gas	
		Expt.	Pred.	Expt.	Pred.	Expt.	Pred.	Expt.	Pred.
0	700	53.98 ±0.65		26.10 ±0.83		5.54 ±0.18		14.25 ±0.01	
	800	52.38 ±0.58		23.09 ±0.88		3.64 ±0.48		20.72 ±0.23	
	900	45.14 ±0.57		13.96 ±0.87		1.04 ±0.27		38.96 ±0.57	
10	700	48.61 ±1.04	49.72	31.24 ±1.02	25.39	6.39 ±0.24	6.66	13.66 ±0.34	17.91
	800	44.84 ±1.98	47.83	30.43 ±0.89	22.80	4.32 ±0.76	3.82	19.47 ±1.03	25.25
	900	42.62 ±1.02	41.08	26.09 ±0.77	13.63	3.13 ±0.20	1.11	27.74 ±1.00	43.26
20	700	47.11 ±0.24	45.46	31.69 ±1.25	24.68	6.23 ±0.24	7.79	13.17 ±1.02	21.15
	800	44.75 ±0.11	43.27	30.13 ±0.35	22.52	5.57 ±0.13	4.00	19.47 ±1.04	29.78
	900	38.81 ±0.45	37.01	24.73 ±0.23	13.30	3.33 ±0.35	1.17	33.07 ±1.22	47.56
30	700	44.06 ±0.24	41.19	31.69 ±1.43	23.98	6.65 ±0.14	8.91	17.44 ±0.23	25.23
	800	39.48 ±0.64	38.71	29.86 ±1.03	22.23	3.42 ±0.27	4.18	27.13 ±1.03	34.30
	900	35.22 ±0.35	32.95	26.08 ±0.45	12.97	1.31 ±0.45	1.24	37.24 ±1.87	51.87
40	700	37.30	36.93	28.04	23.27	6.53	10.03	27.89	28.89
	800	35.12	34.15	24.66	21.94	3.06	4.36	36.92	38.83
	900	29.91	28.88	22.45	12.64	5.82	1.31	41.50	56.17
50	700	32.00	32.67	27.48	22.56	9.09	11.16	30.24	32.55
	800	29.24	29.59	22.63	21.66	3.89	4.54	43.95	43.36
	900	26.90	24.82	20.25	12.31	2.52	1.37	50.16	60.47

The effect of temperature variation on the yields of char, tar and product gas for gasification of coal and coal-corn stover mixtures in N_2 medium (Table 2.6) and CO_2 medium (Table 2.7) were similar to those observed for the corn stover gasification. However, the products yield distribution for the coal biomass mixtures was significantly difference from those of the individual feedstocks, and was expected because the volatile content for corn stover (Table 2.2) is higher than that of coal.

It was hypothesized that because of the high mineral contents of coal (5% ash) and corn stover (9% ash), the combination of the two feedstocks would produce positive synergistic effects and improve gasification of the two feedstocks. However, the presence of these minerals promoted the formation of agglomerates (ash sticking effect) of different sizes and shapes. Agglomerates severely formed at 800°C and 900°C. Photographs of agglomerates of silica sand before and after coal-corn stover co-gasification experiment are shown in Fig. 2.6. Agglomeration phenomenon occurs when alkali species in the ash of feedstock interact with fluidized bed material (silica sand) under high temperature conditions to form low-melting point eutectics. In this study, large chunks of eutectics were collected from the reactor after each experiment and the magnitude of formation increased with increasing corn stover content of the coal/biomass mixture. The eutectic formed was very sticky and required some effort to remove it from the surface of the reactor. Formation of agglomerates may have caused loss of fluidization [11] resulting in poor heat and mass transfer [12] during co-gasification experiments. The gas yields were subsequently lower than predicted (Tables 2.6-2.7). Agglomeration can occur even

when the temperature is below ash fusion point [13] because the presence of K, Na, and Ca compounds lower ash melting temperatures [14, 15], observed defluidization caused by agglomeration when they processed straw in a laboratory-scale fluidized-bed. They also reported that temperature had a significant influence on formation of agglomerates that led to defluidization. They concluded that increase in temperature increased the ash melt and reduced the viscosity of ash melt. In a gasification study, Fryda et al. [16] observed that Giant Reed (*Arundo donax* L.) and Sweet Sorghum had defluidization temperatures of ~790°C and ~810°C respectively. The corn stover samples were rich in potassium and calcium and therefore it was not surprising that these caused considerable agglomeration of the bed material.

Table 2.7. Product yield (dry wt.%) for sub-bituminous coal and corn stover mixtures co-gasification in CO_2 medium.

Biomass ratio (wt.%)	Temp. (°C)	Char		Water		Tar		Gas	
		Expt.	Pred.	Expt.	Pred.	Expt.	Pred.	Expt.	Pred.
0	700	57.30 ±0.87		30.29 ±1.64		5.86 ±0.84		6.30 ±0.59	
	800	48.20 ±0.46		29.03 ±0.81		2.70 ±0.54		18.80 ±1.52	
	900	41.56 ±0.20		26.46 ±1.00		1.05 ±0.17		29.62 ±0.32	
10	700	50.12 ±0.91	53.39	34.93 ±0.32	29.80	4.41 ±0.64	5.92	9.39 ±0.19	10.51
	800	40.24 ±0.32	44.62	33.14 ±0.91	28.53	3.56 ±0.69	2.84	21.24 ±0.59	22.72
	900	37.09 ±1.27	38.39	33.54 ±0.08	26.32	1.89 ±0.06	1.05	27.49 ±1.24	33.00
20	700	47.80 ±0.66	49.48	36.41 ±0.32	29.30	4.51 ±0.22	5.98	11.23 ±0.22	14.71
	800	43.31 ±0.12	41.04	35.46 ±0.78	28.03	2.93 ±0.67	2.98	17.85 ±0.41	26.63
	900	35.42 ±0.98	35.21	33.35 ±0.45	26.18	2.06 ±0.21	1.04	29.12 ±0.34	36.37
30	700	45.32 ±1.02	45.32	32.64 ±0.23	28.80	7.70 ±0.34	6.04	12.98 ±1.23	18.92
	800	40.56 ±0.85	37.45	31.08 ±0.79	27.52	5.88 ±0.65	3.11	22.00 ±0.54	30.54
	900	34.71 ±0.46	32.04	31.39 ±0.54	26.05	2.36 ±0.12	1.04	30.30 ±0.67	39.75
40	700	42.59	41.66	29.16	28.30	7.66	6.11	19.28	23.12
	800	33.24	33.87	29.49	27.02	4.47	3.25	31.55	34.45
	900	30.35	28.87	29.02	25.91	1.32	1.03	38.28	43.12
50	700	36.02	37.75	28.21	27.80	9.19	6.17	26.23	27.33
	800	32.02	30.29	27.34	26.52	4.67	3.39	34.67	38.36
	900	26.10	25.69	28.08	25.77	2.96	1.03	41.74	46.49

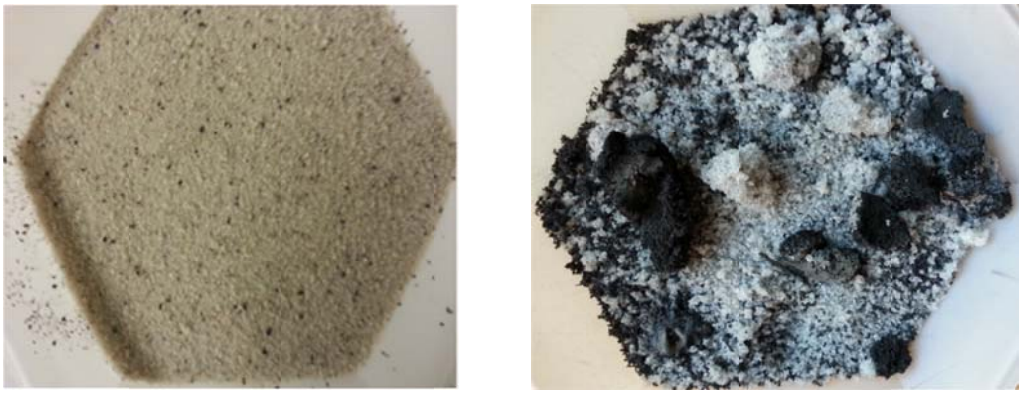

Figure 2.6. Photographs of agglomerates from co-gasification of sub-bituminous coal and 20 wt.% corn stover mixture at 900 ^{o}C. (A) silica sand before experiment and (B) agglomerates of silica sand and char after experiment.

Despite the formation of agglomerates, coal reactivity increased with increasing corn stover content. The char yields for coal-corn stover mixtures were lower than those of single coal. However, no observable synergistic effect between coal and corn stover co-gasification in nitrogen was noted. The experimental product yields were additive compared to predicted values. In Table 2.6, char yields with 10 – 20 wt.% corn stover were 3% to 10% lower than predicted char yields indicating minor synergetic effects. However, minor synergetic effects observed diminished with increasing biomass content and temperature. Similar observations of decreasing interaction between coal and biomass with increasing temperature have been reported [17-19] in separate studies on coal and biomass co-pyrolysis and co-gasification. It was suggested that, active sites responsible for interactions leading to synergies are lost when temperature increases [19].

The liquid yields from the co-gasification experiments were higher than predicted from additive independent reaction of the coal and biomass components of the mixture. In addition, increase in corn stover proportion in coal resulted in increase in tar yields.

The major gaseous products from co-gasification experiments were: H_2, CO, CO_2, and CH_4. Light molecular weight hydrocarbons (C_2-C_4) were present but at very low concentrations. Table 2.8 shows the yield of corn stover gaseous compounds. H_2 and CO were the major compounds produced and their yields increased with increasing temperature. Clearly, there appears to be interaction between coal and corn stover co-gasification on product gas formation, however synergetic effects were not present. The experimental gaseous compounds were either additive or lower than predicted yields except for CO yields in N_2 medium where experimental values were significantly higher at 700°C to 800°C.

The mechanism of coal and biomass interaction leading to synergy has been reported [17, 20].The phenomenon of synergy was theorized as transfer of OH and H radicals from biomass to coal during co-gasification reactions. In this study, up to 36 wt.% of liquid (water) yields were obtained from co-gasification experiments compared to 30 wt.% for predicted water yields. It appears that some of the OH and H radicals produced water instead of interacting with the coal and promoting cracking of aromatic compounds in coal. The concentration of syngas obtained using CO_2 as gasification medium (Table 2.9) were higher (78 vol.% at 700°C, 87 vol.% at 800°C, 93 vol.% at 900°C) than those obtained with N_2 medium (60 vol.% at 700°C, 65 vol.% at 800°C, 75 vol.% at 900°C).

The co-gasification of sub-bituminous coal and corn stover showed that the char reactivity and tar cracking of coal and corn stover mixtures increased with increasing temperature, which led to an increase in gaseous products. Minor synergetic effects and interactions were observed between coal and corn stover char reactivity at 700°C with low biomass content. Coal and corn stover mixtures formed agglomerates of different sizes and shapes at 800°C and 900°C. The agglomeration effect increased with increase in corn stover content of the coal which could potentially limit the coal gasification/corn stover mixture using fluidized bed. H_2 yields obtained were more pronounced at 900°C (41 vol.%) in N_2 gasification medium and 25 vol.% at 700°C in CO_2 medium with 10 wt.% biomass. Overall, syngas (H_2 + CO) concentration was dominant in the product gases especially in CO_2 gasification medium.

Table 2.8. Yield (vol.%) of product gas compounds for sub-bituminous coal and corn stover mixtures in N_2 medium.

Biomass content (wt.%)	Temp (^oC)	H_2	CO	CH_4	CO_2	C_2-C_4
0	700	39.63 ±1.03	18.58 ±1.51	11.57 ±1.03	27.92 ±1.43	2.31 ±0.45
	800	43.12 ±0.97	20.79 ±2.11	9.13 ±0.43	26.37 ±1.98	0.58 ±0.26
	900	48.53 ±1.95	31.80 ±1.84	6.81 ±1.08	12.84 ±1.66	0.02 ±0.00
10	700	24.25 ±2.01	31.23 ±1.94	13.62 ±0.92	27.45 ±2.32	3.44 ±0.65
	800	32.75 ±1.35	31.58 ±1.52	12.29 ±1.08	21.86 ±1.82	1.51 ±0.13
	900	41.00 ±2.28	31.00 ±0.79	9.69 ±1.13	18.08 ±1.01	0.23 ±0.04
20	700	24.96 ±0.53	35.16 ±1.33	12.24 ±2.47	24.59 ±1.87	3.06 ±0.73
	800	30.14 ±1.01	36.31 ±2.45	13.53 ±0.44	18.51 ±2.06	1.51 ±0.33
	900	37.02 ±0.78	35.89 ±1.08	10.99 ±0.53	15.75 ±0.25	0.35 ±0.02
30	700	25.25 ±1.11	36.48 ±2.25	11.40 ±0.01	24.45 ±2.04	2.42 ±0.17
	800	29.93 ±0.43	34.40 ±2.46	12.73 ±0.62	21.50 ±2.19	1.44 ±0.19
	900	35.79 ±2.64	34.99 ±0.32	11.60 ±0.43	17.12 ±0.98	0.50 ±0.04
40	700	26.47	35.96	10.04	24.78	2.76
	800	33.13	34.70	11.02	20.06	1.09
	900	34.49	40.23	10.28	14.70	0.30
50	700	24.49	37.10	9.38	25.78	3.25
	800	27.91	38.87	11.84	19.87	1.51
	900	33.40	39.21	11.63	15.47	0.28

Table 2.9. Yield (vol.%) of product gas compounds for sub-bituminous coal and corn stover mixtures in CO_2 medium.

Biomass content (wt.%)	Temp (^oC)	H_2	CO	CH_4	CO_2	C_2-C_4
0	700	30.52 ±1.46	51.84 ±2.33	12.77 ±0.42	3.13 ±1.27	1.73 ±0.25
	800	28.07 ±1.59	61.16 ±2.18	7.76 ±0.81	2.78 ±0.57	0.22 ±0.05
	900	23.52 ±1.13	69.12 ±0.79	5.85 ±0.17	1.50 ±0.01	0.01 ±0.00
10	700	25.31 ±0.78	51.23 ±2.39	12.90 ±0.83	8.87 ±1.44	1.69 ±0.09
	800	21.29 ±1.72	65.44 ±2.93	8.78 ±0.57	4.07 ±0.52	0.43 ±0.12
	900	20.84 ±2.39	71.86 ±2.69	6.02 ±0.08	1.26 ±0.22	0.02 ±0.00
20	700	24.30 ±1.40	53.42 ±2.27	9.58 ±2.95	11.18 ±0.93	1.52 ±0.13
	800	20.02 ±1.84	53.16 ±3.02	12.00 ±0.45	13.26 ±0.75	1.57 ±0.02
	900	19.25 ±2.11	67.28 ±2.11	6.89 ±1.05	6.35 ±0.77	0.22 ±0.01
30	700	19.25 ±2.02	53.99 ±2.72	12.52 ±0.21	12.08 ±0.14	2.16 ±0.03
	800	19.33 ±1.98	61.36 ±2.88	11.03 ±1.01	7.31 ±1.22	0.97 ±0.01
	900	20.53 ±2.74	63.95 ±2.97	8.50 ±0.74	6.86 ±0.29	0.17 ±0.01
40	700	18.60	51.81	13.14	13.69	2.75
	800	19.61	56.94	12.54	9.96	0.95
	900	20.17	62.68	10.79	6.19	0.17
50	700	18.21	51.21	12.97	15.07	2.53
	800	18.25	59.44	11.86	9.59	0.87
	900	18.82	65.50	11.10	4.42	0.16

Coal and poplar wood co-gasification studies

The co-gasification of poplar wood with coal showed similar trends as the corn stover/coal mixtures except that poplar/coal mixtures did not form any agglomerates when silica sand was used in the fluidized bed reactor. The sub-bituminous coal was blended with poplar wood on weight basis in the proportion of 100:0, 90:10, 80:20, 70:30, 60:40, and 50:50. The product distribution for co-gasification of coal/poplar in nitrogen medium is shown in Table 2.10 and those in carbon dioxide medium are shown in Table 2.11.

Comparison of experimental with calculated data showed that there was no synergistic effect between the coal and biomass and the two feedstocks appeared to gasify independently. In the case of char yield, the experimental results were either higher or agreed with calculated results. Lack of synergistic effect between coal and biomass co-pyrolysis and co-gasification has been reported [21-23]. The yields of tar and product gas exhibited similar trend of non-interaction between the two feedstocks. In the case of 10 wt.% and 20 % wt.% biomass blends, the gas yields appeared slightly higher than the theoretical yields.

Char, water, and tar yields decreased as the temperature increased resulting in increase in product gas yields. The gaseous product and tar yields in co-gasification experiments were higher compared to gasification of single coal. The increased gas production with respect to increasing temperature can be attributed to thermal cracking of tar and high char reactivity as the temperature increased from 700°C to 900°C.

The liquid yields were generally higher in co-gasification of coal and biomass mixtures than in co-pyrolysis. Possibly, the H_2 donated by biomass reacted with CO_2 to produce water based on the reaction: $H_2 + CO_2 = H_2O + CO$. As a result, product gas yields appeared lower in the co-gasification experiments compared with co-pyrolysis results.

The yields of gaseous product components in co-gasification experiments as a function of temperature are represented Table 2.12. The gaseous product was composed mainly of CO and the concentration increased with increasing temperature. The lower yields of H_2 for coal and biomass mixtures confirm the hypothesis that H_2 generated reacted with CO_2 to produce water and CO since the char yields were not affected. The concentration of H_2 and CH_4 were not affected by biomass content of the coal. The concentrations of H_2 and CH_4 remained the same however; CO concentrations increased and CO_2 decreased with increasing biomass content.

The co-gasification behavior of sub-bituminous coal and hybrid poplar wood mixtures using different media (N_2, CO_2) at low temperatures in a fluidized bed showed additive behavior between coal and poplar co-gasification, which indicated lack of synergetic effects. It appeared the two feedstocks underwent thermal degradation independently, which could be attributed to different temperatures of devolatilization for coal and biomass. Furthermore, product gases were composed mostly of syngas. Experiments suggest that high syngas yields can be obtained using CO_2 as co-gasification medium but with poor H_2/CO ratio (≤ 0.6). Nevertheless, H_2/CO ratios increased up to 2.5 with 10 wt.% poplar wood content when steam was used. H_2 yields decreased with increase in hybrid poplar content whereas CO concentrations remained constant or increased with increase in biomass content. In spite of lack of major synergies between coal and poplar, co-gasifying the two feedstocks should be considered a key to a sustainable natural resource management since these mixtures did not form any agglomerates.

Table 2.10. Product yields of sub-bituminous coal and various poplar wood mixtures in a fluidized-bed as a function of temperature and n_2 atmosphere

Biomass content (wt.%)	Temp (^oC)	Char (wt.%)	Water (wt.%)	Tar (wt.%)	Gas (wt.%)
0	700	53.98	26.10	5.54	14.25
	800	52.38	23.09	3.64	20.72
	900	45.14	13.96	1.04	38.96
10	700	51.14	24.00	4.85	19.93
	800	47.50	24.68	2.69	22.73
	900	40.06	4.61	1.12	52.72
20	700	41.48	30.61	2.51	24.59
	800	42.14	19.68	2.01	35.33
	900	37.11	10.94	1.08	50.10
30	700	39.42	24.19	6.52	29.79
	800	34.09	23.08	4.03	38.77
	900	31.53	20.18	2.11	46.01
40	700	32.60	26.22	7.40	33.11
	800	30.62	22.93	4.42	41.81
	900	26.15	19.99	2.14	51.30
50	700	28.91 ±0.23	23.24 ±0.93	7.64 ±0.08	40.00 ±0.25
	800	27.83 ±1.05	19.27 ±0.67	4.29 ±0.03	47.40 ±0.65
	900	21.84 ±0.96	15.73 ±1.03	2.80 ±0.12	59.14 ±1.20

Table 2.11. Product yields of sub-bituminous coal and various poplar wood mixtures in a fluidized-bed as a function of temperature and CO_2 atmosphere

Biomass content (wt.%)	Temp (°C)	Char (wt.%)	Water (wt.%)	Tar (wt.%)	Gas (wt.%)
0	700	57.30	30.29	5.86	6.30
	800	48.20	29.03	2.70	18.80
	900	41.56	26.46	1.05	29.62
10	700	51.07	33.02	4.84	10.51
	800	45.94	32.88	5.32	15.41
	900	39.53	29.96	2.86	27.45
20	700	43.07	32.45	6.97	17.34
	800	41.14	33.51	5.28	19.34
	900	37.15	28.30	2.29	30.49
30	700	42.74 ±1.04	30.39 ±1.32	6.86 ±0.34	19.81 ±0.23
	800	36.21 ±0.18	30.00 ±0.45	5.69 ±0.27	28.00 ±0.16
	900	31.36 ±0.73	29.68 ±0.19	2.72 ±0.23	35.58 ±0.25
40	700	35.50 ±1.19	27.74 ±1.23	8.80 ±0.99	27.36 ±1.23
	800	29.78 ±0.75	26.21 ±0.24	5.29 ±0.23	37.45 ±0.24
	900	26.02 ±0.85	25.01 ±0.32	2.75 ±0.45	46.03 ±0.95
50	700	32.17 ±0.04	26.40 ±0.34	8.30 ±0.34	33.1 ±0.92
	800	24.16 ±0.63	22.41 ±1.01	4.93 ±0.12	48.40 ±1.04
	900	22.09 ±0.56	21.18 ±0.02	2.92 ±0.22	52.83 ±1.02

Table 2.12. Yield (vol.%) of product gas compounds for sub-bituminous coal and hybrid poplar wood mixtures in N_2 medium.

Biomass content (wt.%)	Temp (°C)	H_2	CO	CH_4	CO_2	C_2-C_4
0	700	39.63 ± 2.01	18.58 ±1.73	11.57 ±1.07	27.92 ±0.76	2.31 ±0.20
	800	43.12 ±1.64	20.79 ±1.08	9.13 ±0.71	26.37 ±2.10	0.58 ±0.06
	900	48.53 ±1.29	31.80 ±2.67	6.81±0.09	12.84 ±1.04	0.02 ±0.01
10	700	30.66 ±0.13	30.69 ±2.12	11.11 ±1.51	24.32 ±2.76	3.21 ±1.71
	800	38.46 ±2.05	28.98 ±1.89	12.39 ±1.45	19.37 ±0.22	2.83 ±0.24
	900	43.82 ±1.58	25.31 ±2.96	9.29 ±0.24	18.75 ±1.12	0.79 ±0.09
20	700	29.34 ±1.98	31.96 ±2.68	11.72 ±0.15	25.09 ±2.16	1.89 ±0.28
	800	34.23 ±0.30	35.21 ±2.91	11.76 ±0.65	16.93 ±0.52	1.87 ±0.07
	900	39.17 ±1.53	34.23 ±0.12	10.76 ±0.10	15.54 ±1.19	0.30 ±0.05
30	700	29.42 ±1.32	33.01 ±1.21	11.05 ±1.06	23.74 ±1.77	2.78 ±0.78
	800	34.47 ±1.01	35.45 ±1.67	12.68 ±1.00	16.19 ±2.36	1.21 ±0.11
	900	38.33 ±1.43	32.59 ±2.02	11.28 ±0.98	17.50 ±1.03	0.30 ±0.18
40	700	26.41 ±0.78	34.90 ±1.65	12.08 ±0.63	24.35 ±2.98	2.25 ±1.03
	800	30.32 ±1.23	40.30 ±2.31	12.04 ±1.01	16.07 ±2.34	1.27 ±0.88
	900	34.70 ±2.11	40.13 ±2.10	11.33 ±0.28	13.59 ±1.03	0.25 ±0.07
50	700	23.30 ±1.23	44.64 ±2.31	9.78 ±2.15	19.07 ±1.43	3.22 ±1.21
	800	27.39 ±0.99	43.64 ±2.11	12.06 ±0.96	15.56 ±0.46	1.35 ±0.50
	900	33.48 ±1.76	43.45 ±2.53	10.58 ±1.11	12.12 ±1.53	0.22 ±0.03

Table 2.13. Yield (vol.%) of product gas compounds for sub-bituminous coal and poplar wood mixtures co-gasification in CO_2 medium.

Biomass content (wt.%)	Temp (^oC)	H_2	CO	CH_4	CO_2	C_2-C_4
0	700	30.52 ±1.46	51.84 ±0.03	12.77 ±0.42	3.13 ±1.27	1.73 ±0.25
	800	28.07 ±0.95	61.16 ±2.18	7.76 ±0.81	2.78 ±0.57	0.22 ±0.05
	900	23.52 ±1.13	69.12 ±2.79	5.85 ±0.17	1.50 ±0.01	0.01 ±0.00
10	700	23.39 ±1.84	53.71 ±0.90	14.32 ±0.63	6.89 ±0.42	1.68 ±0.06
	800	21.32 ±0.44	62.73 ±1.98	11.68 ±0.74	3.51 ±0.37	0.74 ±0.09
	900	21.75 ±1.65	68.30 ±2.98	8.09 ±0.53	1.80 ±0.09	0.06 ±0.01
20	700	19.63 ±0.78	52.18 ±2.01	13.71 ±1.21	12.94 ±0.94	1.55 ±0.16
	800	21.65 ±0.71	61.21 ±1.97	11.65 ±0.86	4.91 ±0.31	0.59 ±0.11
	900	22.33 ±0.34	67.58 ±2.18	8.97 ±0.19	0.92 ±0.63	0.19 ±0.22
30	700	18.19 ±0.15	51.03 ±2.22	13.93 ±1.01	13.97 ±0.25	2.88 ±0.15
	800	19.71 ±0.20	57.59 ±2.03	11.95 ±0.45	9.80 ±1.02	0.94 ±0.23
	900	20.78 ±0.11	65.00 ±2.18	9.36 ±1.65	4.69 ±0.83	0.18 ±0.01
40	700	16.05 ±0.43	52.33 ±1.66	12.02 ±1.11	17.04 ±1.05	2.55 ±0.21
	800	17.27 ±0.07	59.75 ±1.88	10.48 ±1.05	11.64 ±0.26	0.86 ±0.34
	900	19.50 ±0.10	67.65 ±2.99	9.76 ±0.68	2.98 ±0.14	0.12 ±1.11
50	700	14.43 ±0.12	54.69 ±0.94	11.12 ±0.74	18.18 ±1.22	2.58 ±0.14
	800	15.75 ±0.32	63.14 ±1.99	9.34 ±0.32	11.13 ±1.09	0.65 ±0.20
	900	17.63 ±1.01	68.86 ±2.11	9.72 ±1.14	3.64 ±1.11	0.15 ±0.03

Gasification of coal and biomass with red mud

Co-gasification of coal/corn stover on red mud results are shown in Table 2.13 through Table 2.16. Product yields (Table 2.13) and product gaseous compounds (Table 2.15) obtained using red mud were all in agreement with predicted yields. This indicated lack of synergistic effect between sub-bituminous coal and corn stover during gasification with red mud catalyst. Experiments with silica sand (Table 2.14 and Table 2.16) showed similar characteristics of additivity between coal and biomass during thermal conversion.

The red mud appeared to promote cracking of char and tars into product gases as their yields were lower compared to those obtained using silica sand. Product gas yields obtained using red mud were slightly higher than product gas yields from silica sand experiments. This could be due to the catalytic effect of red mud compared to silica sand.

The yields of major gaseous compounds (H_2, CO, CO_2, and CH_4) for coal using red mud were different from to those obtained with silica sand. H_2 yields on red mud increased by 56% at 700°C, 31% at 800°C, and 15% at 900°C relative to the silica sand when coal and corn stover (10 wt.%) mixture was gasified using red mud. At 700°C, H_2 concentration increased from 25 vol.% to 39%; at 800°C, H_2 increased from 33 vol.% to 42 vol.%; and at 900°C, H_2 increased from 41 vol.% to 47 vol.%. The CO yields obtained from red mud co-gasification experiments were lower than those from silica sand.

The major effect of red mud co-gasification of coal and corn stover can be seen by comparing the H2/CO ratios for the for the silica sand and red mud gasification products (Tables 2.15 and 2.16). When corn stover was blended with the coal, the H2 production at 700 ^oC was

very high and CO production was relatively and thus the H2/CO ratio was very high (2.0) compared to the silica sand medium where the H2/CO ratio was very low (0.8). In both cases, the addition of 10 wt.% biomass to the coal produced more CO, but in the case of the red mud, there appeared to be simultaneous water gas shift reaction which converted a large fraction of the CO produced to H2 and thus increasing the H2, and CO2 contents while decreasing the CO content as part of the reaction CO + H2O = H2 + CO2. As expected the CO2 content of the gas increased considerably hence the CO2 content of the red mud catalyzed reaction was higher than that for the silica sand reaction. The H2/CO ratio for the coal/corn stover mixture remained almost constant for all temperatures (700, 800, 900 ^{o}C) during the red mud gasification. In the case of the silica sand, the H2/CO ratio increased with increase in reaction temperature apparently because at higher temperatures, biomass gasification produces more hydrogen and thus the increase in the H2/CO ratio.

In the absence of the biomass in the coal, there was strong water gas shift reaction (Table 15) at 700 ^{o}C which generated a high H2/CO ratio (2.9). Under these conditions, the water gas shift reaction was very vigorous, and therefore most of the CO produced from the coal was consumed in the water gas shift reaction. The water gas shift reaction is temperature dependent and reaction rate decreases with increasing temperature hence the decrease in the H2/CO ratio. As the temperature increased the amount of H2 produced decreased because the reaction rate decreased and there were also other competing reactions from the coal that produced more CO as part of the reaction C + CO2 = 2CO.

Thus, for the red mud reaction, in the case of the pure coal, the H2/CO ratio decreased with temperature whereas in the case of the coal/corn stover mixture, the ratio remained almost constant. This is a very important finding because it shows how the addition of biomass to coal using red mud as a catalyst can alter the H2/CO ratio and therefore the gaseous products can be tailored to various applications such as Fischer Tropsch liquids or use directly as syngas for combustion. Additionally, the red mud was able to reduce tar formation in the product gas. Also of noteworthy was the absence of agglomeration reaction in the reactor. The alkali metals in the corn stover did not form any agglomerates with the red mud which makes the red mud an ideal gasification medium for coal and biomass mixtures. These observations encouraged us to submit an invention disclosure for the gasification process.

Table 2.13. Effect of red mud on coal-corn stover co-gasification product yields (dry wt.%)

Biomass content (wt.%)	Temp. (°C)	Char		Water		Tar		Gas	
		Exp.	Pred.	Exp.	Pred.	Exp.	Pred.	Exp.	Pred.
0	700	50.07		31.67		3.26		16.50	
	800	47.31		30.91		2.75		22.66	
	900	43.03		21.29		1.49		40.66	
10	700	47.15	46.73	29.90	30.88	3.58	3.48	17.66	18.92
	800	43.35	43.62	31.39	31.39	2.71	2.70	24.65	24.01
	900	42.21	39.03	20.02	20.52	1.40	1.47	29.40	38.98

Table 2.14. Effect of sand on coal-corn stover co-gasification product yields (dry wt.%)

Biomass content (wt.%)	Temp. (°C)	Char		Water		Tar		Gas	
		Expt.	Pred.	Expt.	Pred.	Expt.	Pred.	Expt.	Pred.
0	700	53.98 ±0.65		26.10 ±0.83		5.54 ±0.18		14.25 ±0.01	
	800	52.38 ±0.58		23.09 ±0.88		3.64 ±0.48		20.72 ±0.23	
	900	45.14 ±0.57		13.96 ±0.87		1.04 ±0.27		38.96 ±0.57	
10	700	48.61 ±1.04	49.72	31.24 ±1.02	25.39	6.39 ±0.24	6.66	13.66 ±0.34	17.91
	800	44.84 ±1.98	47.83	30.43 ±0.89	22.80	4.32 ±0.76	3.82	19.47 ±1.03	25.25
	900	42.62 ±1.02	41.08	26.09 ±0.77	13.63	3.13 ±0.20	1.11	27.74 ±1.00	43.26

Table 2.15. Effect of red mud on coal-corn stover co-gasification gaseous compounds (vol.%)

Biomass Content (wt.%)	Temp. (°C)	H_2	CO	CH_4	CO_2	C_2-C_4	H_2/CO
0	700	41.73	14.47	31.21	10.72	1.87	2.90
	800	43.91	20.23	24.93	10.13	0.80	2.2
	900	47.22	25.67	19.89	7.01	0.21	1.8
10	700	38.68	19.11	28.88	11.18	2.15	2.0
	800	42.38	20.58	25.81	10.16	1.06	2.0
	900	47.35	24.86	18.48	9.16	0.15	1.9

Table 2.16. Effect of silica sand on coal-corn stover co-gasification gaseous compounds (vol.%)

Biomass Content (wt.%)	Temp. (°C)	H_2	CO	CH_4	CO_2	C_2-C_4	H_2/CO
0	700	39.63 ±1.03	18.58 ±0.21	27.92 ±1.43	11.57 ±1.03	2.31 ±0.45	2.1
	800	43.12 ±0.97	20.79 ±0.11	26.37 ±0.98	9.13 ±0.43	0.58 ±0.26	2.1
	900	48.53 ±0.34	31.80 ±1.55	12.84 ±1.66	6.81 ±1.08	0.02 ±0.00	1.5
10	700	24.25 ±2.01	31.23 ±1.94	27.45 ±1.32	13.62 ±0.92	3.44 ±0.65	0.8
	800	32.75 ±1.35	31.58 ±2.32	21.86 ±1.82	12.29 ±1.08	1.51 ±0.13	1.0
	900	41.00 ±2.28	31.00 ±0.79	18.08 ±1.01	9.69 ±1.13	0.23 ±0.04	1.3

3. Modeling of the kinetics of product formation (Klein)

3.1 Methods

3.1.1 Lumped Modeling

Initially, the lumped model strategy was undertaken as a way to understand the chemistry of gasification and lead to more detailed methodologies. As will be discussed, the lumped modeling methodology proved to be the most useful in a number of ways including integration into the CFD modeling and interpretation of experimental findings. The lumped modeling approach began through literature analysis [24-29] of various methodologies wherein the basic form of the model was outlined as such:

Coal → Char + Volatiles + H2O
Biomass → Char + Volatiles + H2O
Char + O2 → CO + CO2 + H2O
Char + CO2 → CO + H2O + H2
Char + H2O → CO + H2 + H2S + N2
Char + H2 → CH4 + H2O + H2S + N2
CO + H2O ←→ CO2 + H2
H2S + CO2 ←→ COS + H2O
CO + H2 ←→CH4 + H2O

For this initial model there was no difference between the Char derived from the Coal lump and the Char derived from the Biomass. The same hold true for the Volatiles. This simplification would have a major impact on the concentrations of the H2S and N2 species as the Char and Volatiles of the biomass would have much different concentrations of the Nitrogen and Sulfur hetero-atoms. If the lumped model were to examine the Biomass species by breaking it down into its three components species (Cellulose, Hemicellulose, and Lignin), then it was thought that the more fundamental chemistry could help guide the reactions and reaction rates. A second pass at creating the model yielded the more detailed lumped network:

Pyrolysis:
Coal → CharCO + Volatiles + H2O
Lignin → CharL + Volatiles + H2O
Hemicellulose → CharH + Volatiles + H2O
Cellulose → CharC + Volatiles + H2O

Gasification:
CharCO + CO2 → CO + H2O + H2
CharL + CO2 → CO + H2O + H2
CharH + CO2 → CO + H2O + H2
CharC + CO2 → CO + H2O + H2

CharCO + H2O → CO + CO2 + H2 + H2S + N2
CharL + H2O → CO + CO2 + H2
CharH + H2O → CO + CO2 + H2
CharC + H2O → CO + CO2 + H2

CharCO + H2 → CH4 + H2O + H2S + N2
CharL + H2 → CH4 + H2O
CharH + H2 → CH4 + H2O

CharC + H2 → CH4 + H2O

CharCO + ½O2 → CO + H2O
CharL + ½O2 → CO + H2O
CharH + ½O2 → CO + H2O
CharC + ½O2 → CO + H2O

CO + H2O ←→ CO2 + H2
2CO + 2H2 → CH4 + CO2
CO + 3H2 ←→CH4 + H2O
CO2 + 4H2 → CH4 + 2H2O
H2S + CO2 ←→ COS + H2O
CH4 + H2O ←→ CO + 3H2
CH4 + ½O2 → CO + 2H2

Combustion:
CharCO + O2 → CO2 + H2O
CharL + O2 → CO2 + H2O
CharH + O2 →CO2 + H2O
CharC + O2 →CO2 + H2O
2CO + O2 → CO2
CH4 + 2O2 ←→ CO2 + 2H2O
H2 + ½O2 → H2O

This network is comprised of 17 separate lumps, and would require 34 reaction rates and 17 material balance ODEs. Whereas the initial model seemed to present the minimum number of lumps, this methodology produced perhaps the maximum number of lumps without delving more into the chemically specific nature of the char and volatile species. Further analysis required the determination of the rate parameters, so another literature review was undertaken to determine "ball park" pre-exponential factors and activation energies. Using the Wiser [30] model of coal, initial guess estimates for the kinetic parameters of the overall lumped pyrolysis reactions for coal were discovered [24], where A = 4.07 x 10^5 s^{-1} and E_a = 27.7 kcal mol^{-1}. However, gasification involves the addition of reactive elements to the pyrolytic reaction set. The presence of carbon dioxide, water, hydrogen and non-stoichiometric amounts of oxygen lead to complexes with the char ring clusters. These complexes then strip the rings of carbon atoms, largely forming carbon monoxide (for oxygen containing reactants), methane (for hydrogen), thereby diminishing the char. This process continues until the char has been completely reacted.

Everson [31] lists the reaction parameters for the carbon dioxide gasification with coal chart in a two-step process. In the initial step, the oxygen complex is created, and a carbon monoxide is emitted. In the second step, the oxygen complex rends a carbon from the char, creating another carbon monoxide molecule:

$$C + CO_2 \leftrightarrow C(O) + CO$$
$$C(O) \rightarrow CO$$

A Lanmuir-Hinshelwood equation was constructed with the following form:

$$r_1 = \frac{k_2 K_{CO_2} P_{CO_2}}{1 + K_{CO_2} P_{CO_2} + K_{CO} P_{CO}}$$

$$k_2 = k_2^0 exp\left(\frac{-E_2}{RT}\right)$$
$$K_{CO_2} = K_{CO_2}^0 exp\left(\frac{-H_{CO_2}}{RT}\right)$$

	E_1 (kcal mol^{-1})	E_2 (kcal mol^{-1})	H_{CO2} (kcal mol^{-1})
Coal-Char A	22 (+/- 2)	26 (+/- 3)	3 (+/- 1)
Coal-Char B	23 (+/- 2)	33 (+/- 3)	11 (+/- 1)

Similarly, reaction with H_2O is given as a two-step process:

$$C + H_2O \leftrightarrow C(O) + H_2$$
$$\mathrm{C(O)} \rightarrow \mathrm{CO}$$

which leads to a Langmuir-Hinshelwood expression:

$$r_2 = \frac{k_4 K_{H_2O} P_{H_2O}}{1 + K_{H_2O} P_{H_2O} + K_{H_2} P_{H_2}}$$
$$k_4 = k_4^0 exp\left(\frac{-E_4}{RT}\right)$$
$$K_{H_2O} = K_{H_2O}^0 exp\left(\frac{-H_{H_2O}}{RT}\right)$$

	E_3 (kcal mol^{-1})	E_4 (kcal mol^{-1})	H_{H2O} (kcal mol^{-1})
Coal-Char A	34 (+/- 3)	51 (+/- 3)	16 (+/- 2)
Coal-Char B	24 (+/- 2)	49 (+/- 3)	24 (+/- 2)

Many gasifier units use combustion as an energy source. The bottom layers of material are fed with a stoichiometric amount of oxygen allowing for complete oxidation and combustion of the coal. The products of combustion and excess oxygen then bubble their way up through the bed, providing the reactive gases necessary for the gasification process. Williams [32] lists the overall reaction parameters for the combustion of different types of coal chars, shown in Table 3.1. While the activation energies fall within a small range, the pre-exponential factors show the properties of diffusion effects and wetness of the coal. Although the terms have been listed for coal, they provided a starting point for the consideration of biomass as well.

Table 3.1 Reaction parameters for coal chars [32].

	E_a (kcal mol^{-1})	A (kg m^{-2} s^{-1} Pa^{-1})
Thoresby	38.0	9.5
Pittsburgh	36.3	15.3
Asforby	38.5	53.6
Betts Lane	37.0	2.12

3.2 Molecular-level modeling

3.2.1 Background on molecular-level modeling

Molecular level modeling capitalizes on the specific chemistry of a reaction system to predict the products based on the structural breaking and formation of atomic bonds that take place during reaction. Whenever a molecular-level model is to be employed, four stages of development need to be undertaken:

- The feed must be described molecularly
- The reaction network must be constructed
- The balance equations must be solved, and the rate parameters tuned
- The properties of the effluent must be predicted

3.2.2 Molecular structures

Molecular-level modeling differs from lumped modeling in that each species within the reacting system is considered as an individual molecule. For most light gas products this is straight forward, we can determine the structure of the species and represent it individually on the computer. However, complications arise for the large solid species being handled by this gasification chemistry. For instance, coal as a molecule has nearly infinite configurations, but in order to perform molecular level chemistry, we must have a governing structure. Therefore, we created a new single species for each of the solid species that encompasses the prevalent structural moieties of the solid.

3.2.3 Reaction *network* construction

After selecting the representative structural molecules for the solids, efforts turned to understanding the chemistry of reaction from a molecular pathways point of view. Broadly, there are four categories of reaction in our system:

- Drying
- Pyrolysis
- Gasification
- Gas Shift Reactions

The drying reaction is simply the removal of physically bound water from the feed solids (coal and biomass). As such there is no chemical bonds being broken, but the reactions themselves can be written as:

wet coal → coal
wet lignin → lignin

For the sake of simplicity, we assumed that the physically bound water in the biomass was physically bound to the lignin. The rate of drying reactions is much greater than any other reaction family, so it was assumed this would not skew the results. Pyrolysis was modeled in this system through the breakdown of appropriate single bonds. For coal and lignin, this amounts to the separation of aromatic ring structures from one another through dealkylation.

In pyrolysis cellulose and hemicellulose underwent ring opening and side chain cracking operations that converted the polymers into tar type products:

$cellulose_x$ ←→ *x* levoglucosan
$cellulose_x$ ←→ *3x* glycolaldehyde
levoglucosan ←→ *2* methylglyoxal + H_2O
methylglyoxal + H_2 ←→ acetol
acetol + H_2 ←→ propylene glycol
propylene glycol + H_2 ←→ isopropanol + H_2O
levoglucosan ←→ 6 carbon + H_2O

For the gasification, reactions occurred when the CO_2, H_2O, H_2, and possible trace amounts of O_2 reacted with the heated fuel, char and tar. These reactions were largely represented through the breakdown of the aromatic rings [33]:

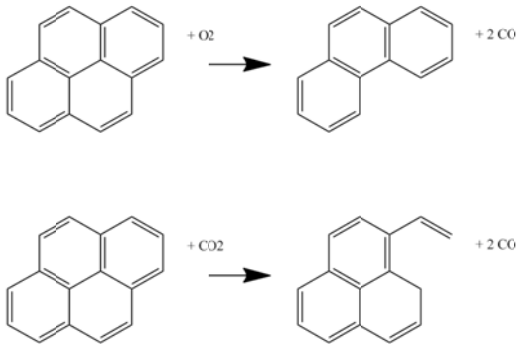

Finally, the gas shift reactions were explicitly represented as:
CO + H2O ←→ CO2 + H2
CO + 3H2 ←→CH4 + H2O
CH4 + H2O ←→ CO + 3H2

This set of reactions created thousands and thousands of individual species, mostly in the Tar and Char fractions. Upon interacting with the CFD team, it was made clear that having hundreds of species, much less thousands, led to impossibly long code calculations. As the integration of the kinetic ODEs into the CFD model was meant to be a keystone for this project, the pursuit of further elucidating the molecular level model was abandoned and alternatives were sought.

3.3 Attribute reaction modeling

3.3.1 Feed modeling with ARM

One such alternative to straight-forward molecular-level modeling, was the use of attribute reaction modeling (ARM) [34]. Originally included in the proposal, attribute reaction modeling is a method for reducing the number of ODEs, reactions, and parameters for a system by dividing a species up into finite sets of attributes.

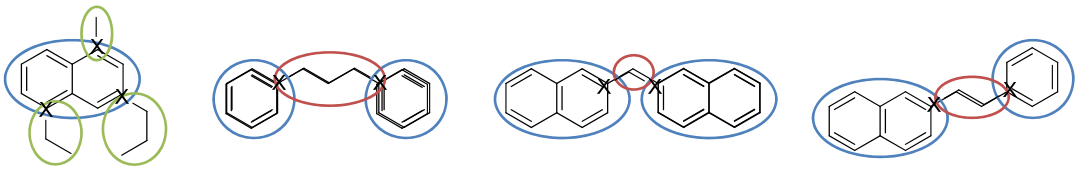

These attributes fall into three categories:

Cores – Largely defined as rings or closely bound ring clusters

Side Chains – Paraffinic or olefinic chains that lead from cores, but do not connect to other cores

Inter-unit Links – Paraffinic or olefinic chains that lead from cores, and do connect to other cores

After breaking down the structures into attributes, there were on the order of 17 (O(17)) unique cores, O(28) unique inter-unit links, and O(12) unique side chains among the feed species. Before reaction analysis could take place, our group decided to switch from the Wiser model of coal to the Shinn model of coal so as to converge research efforts into the thermal degradation of coal without our group. The shift to the Shinn model produced O(31) cores versus the O(13) in the Wiser model; O(8) inter-unit links versus the O(13) in the Wiser model; and O(12) sidechains versus the O(5) in the Wiser model.

3.3.2 Reaction network generation with ARM

Within the ARM framework, each attribute was reacted independently in the kinetic model. The number of reactions for reaction family for each species type was reported. However, when dealing with the kinetics, the tens of thousands of possible species would not need to be considered. Instead, only the initial attributes and their post-reaction counterparts ever need to be considered. This lead to a dramatic reduction in the number of ODEs necessary, which in turn meant quicker calculation time. However, the CFD calculations need to take place on single species (with readily available properties). This meant that the entire set of species would need to be reconstructed on the fly in line with the CFD time steps. Again, this would tax the simulation beyond the point of utility. In addition, in order to correctly predict the initial concentrations of the attributes within the feed, more data was necessary than the Ultimate and Proximate analysis of the coal and biomass provided. For these reasons, the ARM method was also abandoned, and in its place efforts were turned toward new lumped modeling schemes.

3.4 Results

3.4.1 Advanced lumped modeling background

One of the key abstract concepts that was established during this project was the integration of the experimental, kinetic modeling, and fluid dynamics modeling programs. From the kinetics point of view, molecular based modeling, though possible, produced too many species and equations for the CFD simulation to handle practically. ARM modeling was limited by a lack of analytical property data for establishing the concentrations of the initial attributes, an overabundance of attribute species (though much lower than straight forward molecular modeling), and the needs of the CFD simulation to rebuild the attributes into actual species at each time step.

On the other hand, the traditional lumped modeling outlined earlier, produced a reasonable number of species and equations for the CFD team, but lacked detail within the gas lump. As

this was a good starting point for the establishment of a model that could be used by the CFD team, a series of models were outlined to determine the optimal model for interaction

3.4.2 Establishing an optimal lumped model for CFD integration

In trying to integrate any of the previous models into the CFD scheme, it was discovered that the reactions themselves would need to have more stoichiometric and mass balance detail than what was being provided by the previously proposed lumped kinetic scheme. Establishing a molecular weight for coal, a “mole of coal” was a hard subject to quantify because of the seemingly infinite matrix that makes up coal, but we looked at the various structural models of coal, and determined approximately what an independent active center might look like. Assumptions were made based on the character of the resultant products of our experimental gasification (like the lack of sulfurous compounds).

This active center of coal is composed of three major attributes: an aromatic cluster, a section of saturated rings, and a set of side chains (Fig. 3.2). The pyrolysis of the coal due to high temperatures will crack off the single bonds and break open the saturate rings, leaving centers of aromatic rings as the char. The aromatic cluster, in turn, can be conceptually decomposed into active centers for gasification reaction (Fig. 3.3). The gasification reagents will attack the outer most portions of the unit sheet of rings and whittle their way into the center atoms.

3.4.3 A new semi-molecular paradigm in lumping

Ultimately, even though the previous models tried to capture a sense of the stoichiometry of the reactions, the CFD simulation required a more physically explicit and elementally balanced set of equations. Turning from the lump-to-lump kinetics, we attempted to establish a stoichiometricly balanced single reaction equation for each of the steps in the gasification process. A further review of the literature led us to the work of Xu and Qiao [35], which in turn led back to the works of Bradley, Lawes, Park and Usta [36], and Merrick [37].

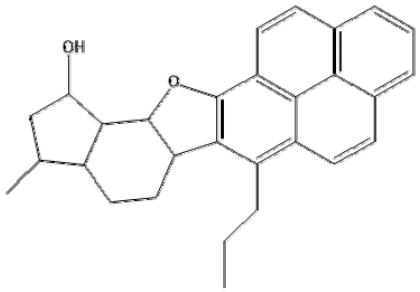

Figure 3.2. An active center of coal

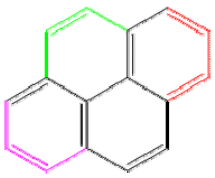

Figure 3.3. A post-pyrolysis char "molecule" with highlighted active centers

3.4.4 The final model

One last set of changes were required by the CFD team. The penultimate form of the model was based on a PFR and used the common assumptions and simplifications common to that reactor design. As such, the balance equations were written in terms of flow rather than concentrations. In addition, Because of the nature of the ultimate and proximate analyses, the model used mass rather than moles so as to not require the establishment of molecular weights for the solids. A change in both of these factors was requested. As such, the model was rewritten so that the rate laws provided concentration compatible changes. Among other factors, this meant that the random pore model needed to be dropped, and the K_p, partial pressure equilibrium constants that were calculated based on the enthalpy and entropy of reaction, needed to be converted to K_c, molar concentration equilibrium constants. Calculating molecular weights for the gases was straight forward. The char was assigned a value of 12 so as to provide mass balance to the gasification reactions. The tar was assigned an average molecular weight of 182 based on a weighted analysis of commonly reported compositions. Coal's molecular weight was chosen to be an average value of 1000:

Drying – the release of moisture trapped within the wet coal into steam:

1) Moisture → H_2O
   $r_1 = k_1 C_{Moist}$
   where, $k_i = A_i e^{-Eai / RT}$ and C_i = the molar concentration (mol/L) of species i

Devolatilization – the removal of volatile compounds from the dry coal leaving char and ash in the solid phase

2) Coal → 44.38 Char + 0.76 CH4 + 1.18 CO + 2.53 CO2 + 1.44 Tar + 2.09 H2O + 5.57 H2
   $r_2 = k_2 C_{Coal}$

Gasification – The heterogeneous removal of carbon from the solid char into the gas phase through three different gasification reactant gases: steam, carbon dioxide, and hydrogen.

3) Char + H2O → CO + H2
   $r_3 = k_3 C_{Char} C_{H2O}$
4) Char + CO2 → 2CO
   $r_4 = k_4 C_{Char} C_{CO2}$
5) Char + 2 H2 → CH4
   $r_5 = k_5 C_{Char} C_{H2}$
   Note that it is not C_{H2}^2

Gas Phase Reactions – Consists of two reversible gas phase equilibrium reactions, CO Methanation and Water-Gas Shift

6) CO + 3 H2 ←→ CH4 + H2O
   (at the conditions of the experiments, the equilibrium is shifted heavily towards the left)
   $r_6 = k_6 C_{CO} C_{H2}^3 – C_{CH4} C_{H2O} / Keq_6 (RT)^2$
   $Keq_i = e^{\Delta Si/R – \Delta Hi/RT}$
7) CO + H2O ←→ CO2 + H2
   $r_7 = k_7 C_{CO} C_{H2O} – C_{CO2} C_{H2} / Keq_7 (RT)^0$

Tar Condensation – the conversion of the tar species into gas and char

8) Tar → 14.3 Char + 0.5 CH4 + 0.7 H2 + 0 CO
   $r_8 = k_8 C_{Tar}$

Even without the random pore model, the tuning of the rate parameters went well and produced the following results and parity plots, shown in Table 3.2 and Fig. 3.4.

Table 3.2. Arrhenius parameters for the final, molar concentration based, lumped model

Reactions	lgA	E (kcal/mol)	dS	dH
Drying	10.98	54.34		
Devolatilization	0.78	10.76		
Steam Gasification	8.69	45.24		
CO2 Gasification	-2.26	-8.94		
H2 Gasification	-2.53	-8.62		
Methanation Shift	1.99	41.68	-0.06055	-54.168
Water Gas Shift	8.82	40.00	-0.00768	-8.400
Tar Condensation	2.38	17.61		

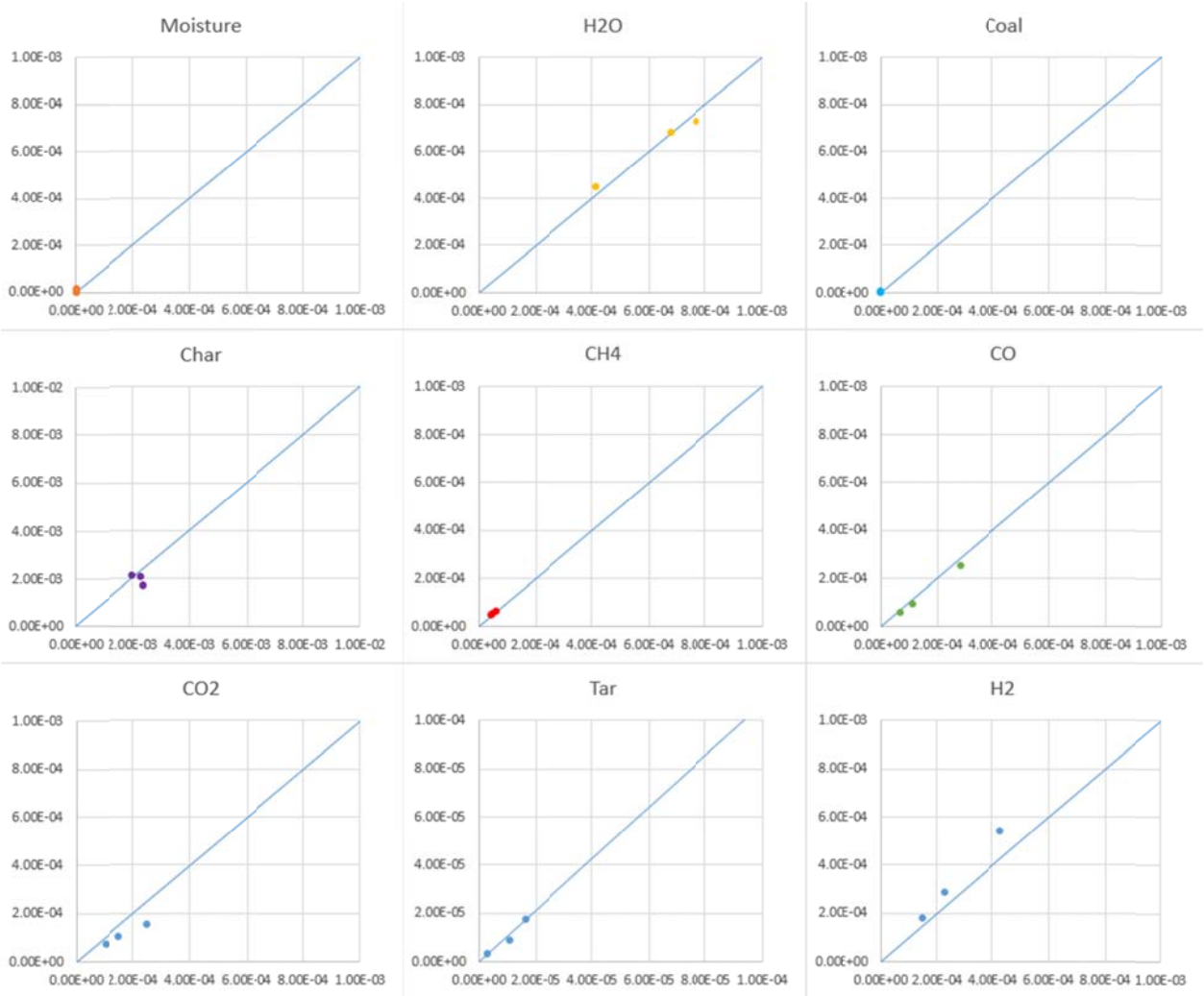

Figure 3.4. Parity plots for the final, molar concentration based, lumped model

4. Efficient methods for solving reactions (Sheikhi)

4.1 Methods

In this part of the project, our research was focused on efficient implementation of multi-phase chemical kinetics in the Multiphase Flow with Interphase eXchanges (MFIX) code (developed by NETL). A new interface was developed that facilitated implementation of various chemical mechanisms in MFIX. The interface allows splitting the hydrodynamics and chemistry calculations into separate fractional steps to improve flexibility and computational efficiency of each solver. To show the performance of MFIX coupled with the interface, we conducted simulation of various multi-phase flows in fluidized bed gasifiers.

Understanding the physical process underlying fluidization is precursor to providing a reliable account of chemical kinetics. Therefore, we concentrated on understanding the dynamics of fluidization and providing reliable prediction of mixing in fluidized beds. In particular, the influence of numerical error on fluidized bed simulations was one focus area addressed due to the important role that numerical diffusion plays on the accuracy of capturing bubble dynamics, which significantly affects gas-solid mixing and reaction processes.

Simulation of gas-solid flows was handled using an Eulerian-Eulerian method, also known as two-fluid modeling (TFM). The model is based on the assumption there are enough solid particles in the system that the multiphase mixture can be considered to be interpenetrating continua. In TFM, each computational cell is assumed to contain individual phases as continuous media, each occupying a fraction of the volume. The equations governing are the compressible form of continuity and momentum for each phase. In this work, physical properties for phases are assumed to be constants. Closure models for these equations are described in previous studies, e.g., Refs. [38-40].Numerical simulations are performed using MFIX, which is based on finite volume discretization using a staggered grid arrangement. To study the influence of numerical error, various discretization schemes were considered: first order upwind (FOU), which is meant to generate large numerical diffusion; higher-order flux limiter schemes such as Superbee and Monotonized Central (MC); Deferred Correction (DC) and Downwind Weighting Factor (DWF) methods. Simulations were performed using a wide range of grid resolutions to study the effect of mesh resolution on the results.

Efficient implementation of chemical kinetics was another major area of focus in this study. Due to the structure of MFIX, consideration of chemical mechanisms with various levels of complexity has been challenging and prone to issues. For this purpose, a new reaction module was developed, serving as an interface to facilitate implementation of mechanisms. The module, entitled MCHARS (Multiphase Chemistry And Reaction Solvers) is coupled with MFIX. This coupling requires modification of the following MFIX original files: *usr_mod.f, mchem_init.f, react.f, physical_prop.f, mfix_l.make*. To understand these modifications, it is useful to explain chemical reaction implementation in MFIX.

The first method involves *rrate.f*, in which reaction rates rate are defined. Heat release source terms are hard-coded for each chemical mechanism. The chemical reaction is solved with hydrodynamic equations using a time step size dictated by the numerical stability condition or reaction time scale. For fast reactions with very small time scales, this can result in a prohibitively large number of time steps. The second method considers chemical reaction integration at a separate step from the hydrodynamics equations. Implementation of this method uses *mchem_mod.f,* which allocates the global variables. The subroutine *mchem_odepack_init.f* sets the values of the control parameters for ordinary differential equation (ODE) solver; *physical_prop.f* sets the physical and thermodynamic variables; and *fex.f,* assigns the reaction rates and source terms. The latter, requires hard-coding, which is subject to bugs and mistakes. As an alternative, MCHARS provides a self-contained reaction module, handling all thermodynamics and chemical reaction calculations. Reaction mechanisms are defined as additional plugins; MCHARS provides chemical and heat release source terms automatically

and handles their integration using various stiff ODE solvers. Other modifications to MFIX include (1) c_p values for different species in include files as a function of temperature. In MCHARS, specification of thermodynamic data and all corresponding calculations are handled and there is no longer need for such include files; (2) heat release and reaction source terms needed to be computed *a priori* and hard-coded in fex.f. In MCHARS, all source terms are automatically calculated; (3) some c_p values were redundantly hard-coded in the physical_prop.f. All specifications are done consistently in MCHARS; (4) chemical reaction source term Jacobian needed to be provided in *G_derives* subroutine, which is generally not available for various mechanisms. In MCHARS, Jacobian is calculated numerically by stiff ODE *solver;* (5) calculations of transport properties (e.g. Sherwood number) were done in user-defined subroutines. In MCHARS, transport properties are consistently handled.

4.2 Results

4.2.1 Numerical Schemes

Our initial study was focused on studying the effect of numerical discretization schemes on accurate prediction of fluidization in fluidized beds. The importance of this study is because of the role of bubble dynamics in gas-solid mixing and its subsequent influence on chemical reaction. It has been demonstrated [41] that accuracy of numerical schemes has a significant effect on capturing bubble formation and advection. The flow configuration is a fluidized bed reactor studied experimentally by Agblevor's group. The reactor is a cylinder with inner diameter and height of 5.08 cm and 30 cm, respectively. Nitrogen gas is fed into the reactor from the base of the distributer plate with uniform velocity and discharged is to the atmosphere at the top. A bed of coal particles (Geldart A classification) is considered within the reactor with the initial height of 1.351 cm, which is set to correctly predict the experimental pressure drop inside fluidized bed. The reactor is simulated using a two-dimensional (2D) Cartesian mesh in a rectangular domain corresponding to the central plane of the cylindrical geometry. The effectiveness of such domain to obtain quantitative prediction of bubbling regime in fluidized beds has been demonstrated in previous studies by Battaglia's group [42, 43]. Boundary conditions include uniform velocity at the inlet, atmospheric pressure at the outlet, no-slip boundary condition for gas-wall interaction and partial-slip boundary condition for particle-wall interaction (Johnson-Jackson partial slip boundary conditions) on left and right boundaries. To capture the bubbles correctly, higher order discretizing methods (with TVD numerical schemes) and fine mesh sizes (about 10 particle diameters) has been used. These are the Superbee and MC schemes with DC and DFW algorithms.

To validate MFIX predictions of fluidization with the experimental data, Fig. 4.1 shows the pressure drop versus inflowing gas velocity. Initially, by increasing inlet gas velocity, experimental fluidization shows semi-linear behavior for pressure drop up to the minimum fluidization velocity (U_{mf}=8.22 cm/s) as predicted by the Ergun equation. As shown, MFIX provides accurate prediction of pressure drop at the fluidized state using various numerical schemes.

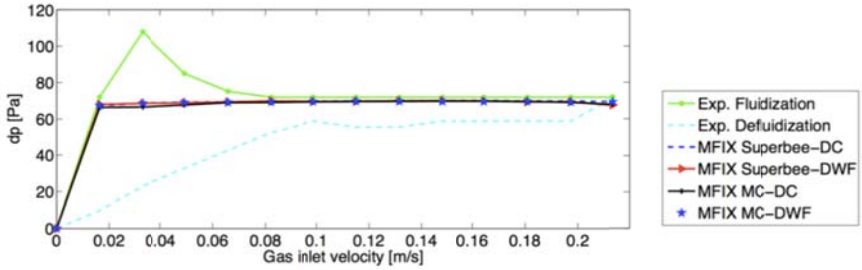

Figure 4.1. Averaged pressure drop versus gas velocity along axis in coal fluidized bed.

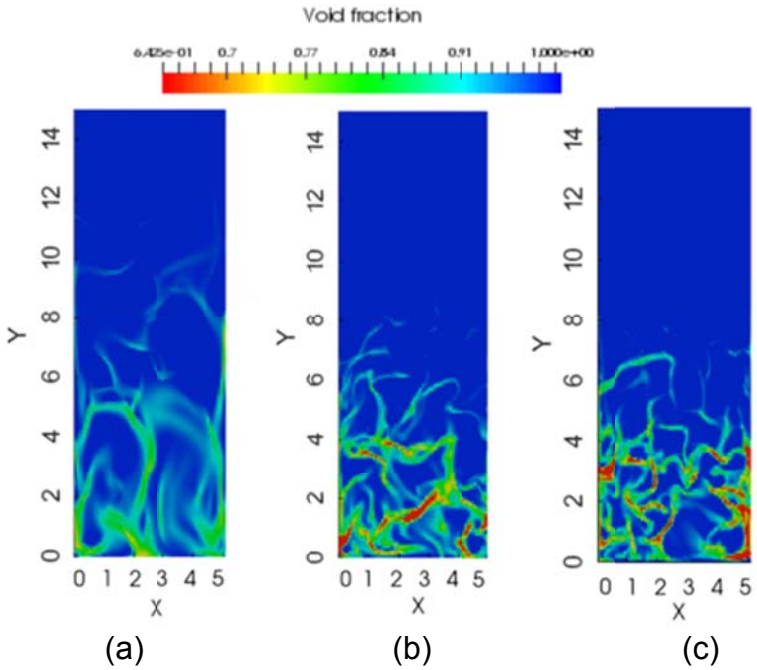

Figure 4.2. Instantaneous void fraction contours in a coal fluidized bed with the superficial velocity of $U_g = U_{mf}$ 2.6 and different schemes: a) FOU, b) MC (t=0.17s), and c) Superbee.

To get an estimate of bubble location, shape and size, MFIX results are analyzed at time t=10 s. Void fraction contours are shown in Fig. 4.2 to compare predictions obtained from FOU, MC and Superbee schemes are depicted. As shown, with non-TVD schemes, such as FOU, the solid gas interface is overly smeared due to their excessive numerical diffusion as also discussed. Simulations obtained from higher order TVD schemes, such as MC and Superbee, show better prediction of the discontinuity at the solid gas interface. Besides, capturing the interface the numerical diffusion affects the shape and size of the bubbles.

The pressure drop profile along the bed (Fig. 4.3) shows that the pressure increases with the depth in the dense phase and remains constant in the free board. The near constant pressure drop at small y values occurs within bubbles from which the width of the bubbles can be determined. Near y=0 the pressure drop shows a drastic increase in the region below the bubbles. Consistent with Fig. 4.2, Fig. 4.3 shows that by applying TVD schemes, bubbles are almost round in shape, while non-TVD schemes predict elliptical shaped bubbles. The round shape of bubbles is due to less numerical diffusion associated with Superbee and MC methods. Figure 4.3 illustrates that the excessive numerical diffusion of the FOU scheme leads to increases pressure drop and more uniform distribution of particles in the radial direction from the centerline to the wall (i.e., formation of particle clusters). This scheme also shows less pressure drop at the wall. The TVD schemes, on the other hand, exhibit larger pressure drop near the wall due to formation of vortical structures. As a characteristic of fluidization, in Fig. 4.4, the time averaged void fraction profile along the central axis of the bubbling bed is shown. The gas entering the reactor fluidizes the dense bed, which results in circulation and bubble formation. The bed expands causing decreased void fraction in the vertical direction, eventually approached unity (gas phase) in the freeboard. In Fig. 4.4, it is observed that large numerical diffusion with FOU causes wider particle distribution and thus larger void fraction near the bottom of the bed. It also leads to excessive increase in the bed height. As shown in these figures, TVD schemes with flux limiters give almost similar prediction of void fraction profile and bed height.

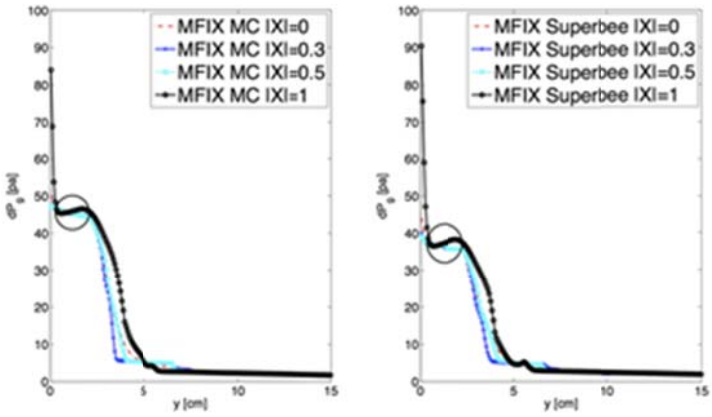

Figure 4.3. Instantaneous gauge pressure along coal fluidized bed at t=0.3 s with of $U_g = U_{mf}$ 2.6 using Superbee (left) and MC (right) schemes. |X| denotes the normalized radius from the centerline. The circles indicate the bubble region.

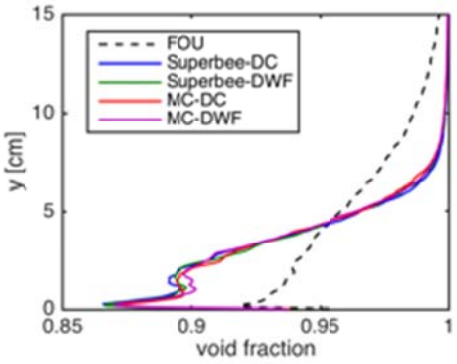

Figure 4.4. Time averaged void fraction profile along coal fluidized bed at $U_g = U_{mf}$ 2.6.

4.2.2 MCHARS Module

Another component of the work involved extensive assessment of MCHARS with the results obtained using original MFIX and validation against experimental data. The former was to assure MCHARS could reproduce the original MFIX results. Two reacting simulations from the MFIX 2012 tutorials were used: silane deposition and coal combustion. The silane deposition case was originally implemented in MFIX in prior studies of Battaglia's group via fractional steps method [44]. We conducted MFIX simulations to obtain instantaneous and time-averaged data for assessment of MCHARS. The original MFIX results are compared with coupled MFIX-MCHARS. Some comparisons are shown in Fig. 4.5. As shown, MCHARS and MFIX results are practically indistinguishable even instantaneously. This is an indication of good performance and correct implementation of MCHARS.

Further assessment of MCHARS considered coal combustion in a spouted bed. In the original MFIX, reactions are implemented in the *rrates.f* subroutine. The reaction source term is linearized and solved along with the species transport equations. Given the very small time steps associated with chemical reactions, the time step for integration of all transport processes adapt to that of the species. As result, the rate of convergence is extremely slow, causing the computational time to increase significantly. The situation becomes more challenging as the stiffness of reaction mechanisms increases, for example, in catalytic reactions. To remedy this problem, the fractional steps method is proven to be useful to separate integration of the

chemical reaction into a separate module. Using this approach the transport equations are integrated with the flow time scale and the integration of chemical reaction is handled using a standard stiff ODE solver. Coal combustion provides a strict case to assess the MCHARS performance and compare with original MFIX, which uses a different integration scheme and different implementation to account for heat release. Some results are presented in Fig. 4.6 comparing MFIX with MCHARS-MFIX. As shown, there are very close agreements between the predictions obtained from the two codes, despite their major differences. The small deviation between the results is inevitable due to round-off error at long simulation times.

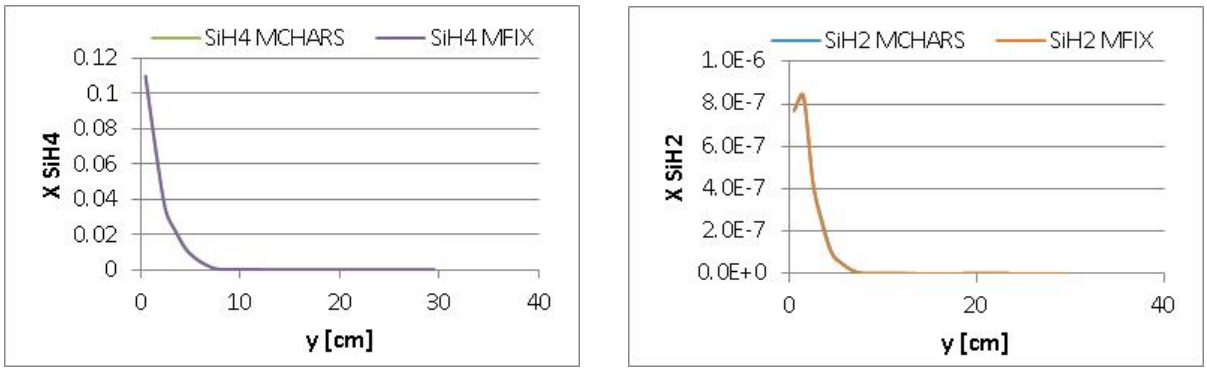

Figure 4.5. Prediction of SiH4 and SiH2 mass fraction using the reaction module (MCHARS) and the original MFIX.

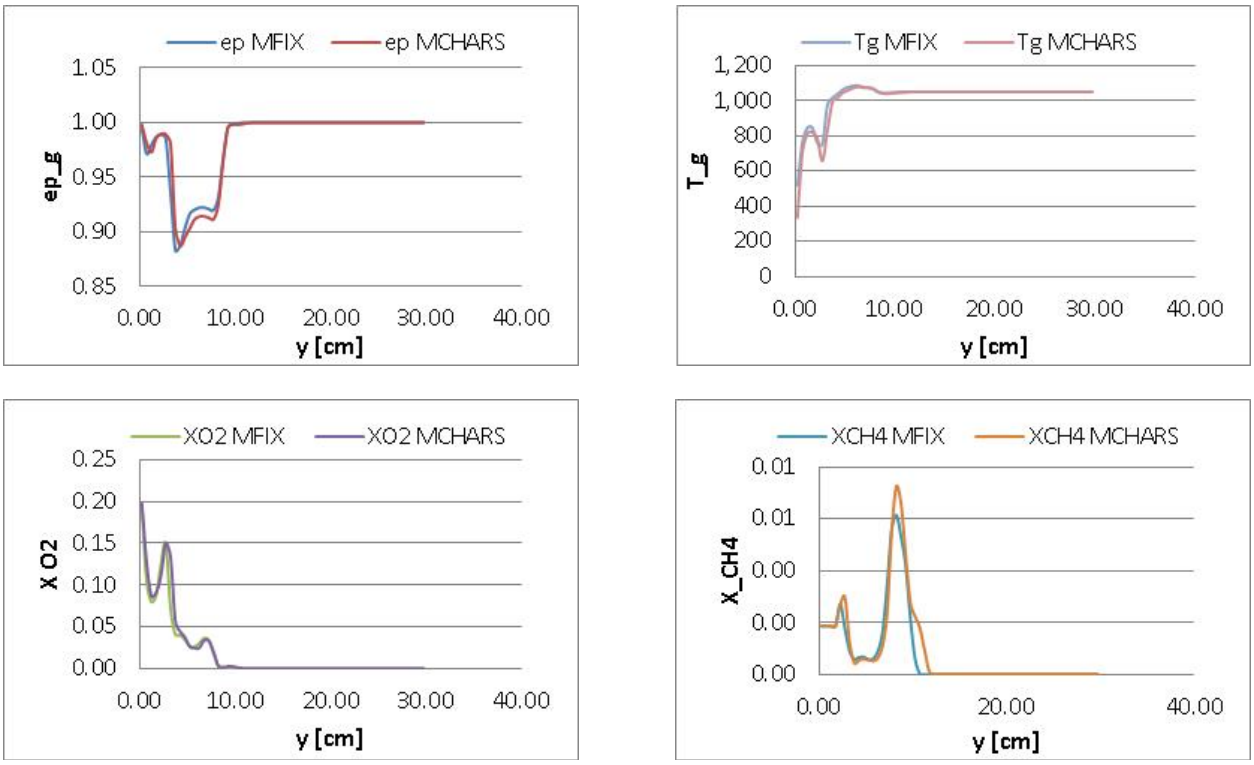

Figure 4.6. Prediction of void fraction, temperature, and oxygen and methane mass fractions using the reaction module (MCHARS) and the original MFIX.

In continuation of this work, we performed simulation of coal gasification in a fluidized bed. The objectives are (1) to assess the accuracy of coupled MFIX-MCHARS against experimental data, and (2) to provide understanding of coal gasification through computational fluid dynamics (CFD) simulations. The test case [39] is a reacting bubbling bed reactor with 10 cm diameter and 30 cm height. To reduce slugging, the expansion section is added with 14 cm diameter and 20 cm height. Figure 4.8 shows a schematic of the reactor. The bed is initially filled with inert matrix (25% limestone and 75% silica by weight), which is fluidized by air flow. Coal (Kansas bituminous) enters the reactor by gravity through a vertical feed pipe (3 cm in diameter) from the top and is discharged at a location about 8 cm above the static bed. A purge flow of nitrogen aided solid flow through the feed pipe and prevented gas backflow. From the bottom of the reactor steam is introduced into the bed. The gas exiting the reactor passes through a cyclone to remove solid particles, e.g., char from the gas stream. The MFIX input parameters used are listed in Table 4.1 and the chemical mechanism [45] parameters are given in Table 4.2. Next, we present some of the results from these simulations.

Table 4.1. Simulation parameters.

Exp. No.	1
Feed	
Coal feed [g/s]	0.073
Steam supply [g/s]	0.147
Operating pressure [atm]	1.0
Entrance temperature [K]	400.0
$A_c[cm^2/g]$	13,130.0
$\rho[g/cm^3]$	2.608
Bed	
Operating temperature [K]	1073.0
ϵ_{mf}	0.43
$u_{mf}[cm/s]$	12.0
$m_{inert}[g]$	973.0
$m_{coal}[g]$	0.068
$\rho_{bulk}[g/cm^3]$	1.58
$u_o[cm/s]$	16.5
$d_p[cm]$	0.0297
$h_0[cm]$	10.0

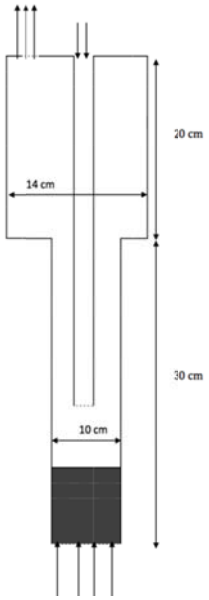

Figure 4.8. Schematic of the gasifier.

Table 4.2. Chemical reaction (Arrhenius)

No.	Reaction	Activation energy ($E_i[kJ/kmol]$)	Frequency factor (K_{ir}^0)	Equivalence ratio ($K_{eq} = K_{Fi}/K_{Bi}$)
1	$C + H_2O \xrightarrow{k_1} CO + H_2$	121,417	5.0e2 [m/hr]	
2	$C + CO_2 \xrightarrow{k_2} 2CO$	360,065	2.0e8 [m/hr]	
3	$C + 2H_2 \xrightarrow{k_3} CH_4$	230,274	7.5e7 [m/hr]	
4	$CO + H_2O \underset{k_5}{\overset{k_4}{\Longleftrightarrow}} CO_2 + H_2$	12,560	1.0e7 $[m^3/kmol.hr]$	$0.0265exp(3955.7/T)$

Figure 4.9a shows the contours of void fraction within the bed. Coal enters the bed from the central pipe and mixes with limestone and silica as the bed goes through intense bubbling. The height of the bed rises at the left side where the gas-solid mixture exits the domain. The bubbles formed during fluidization in the bottom and become elongated as they move downstream. The reactor has an expansion zone that helps reduce slugging in the bed, especially near the outlet. Higher solids fraction near the outlet gives the chance of char gasification near the left wall, leading to increased CO and H_2 mass fractions at the outlet as shown in Fig. 4.9. Due to the chemical reactions, species CH_4, CO, CO_2 and H_2 are produced in the reactor following coal gasification process. It is observed that CO has higher values than CO_2, which is caused by the water-gas shift and char gasification reactions, as they occur simultaneously. CH_4 concentration along the bed shows that the methanation reaction is the rate limiting reaction. Higher mass fractions of CO_2 and H_2 next to the left wall is caused by the water-gas shift reaction in which the forward reaction becomes more dominant than the backward one in that region. The behavior is consistent with the void fraction contours, which shows presence of coal and thus chemical reaction activity near the outlet.

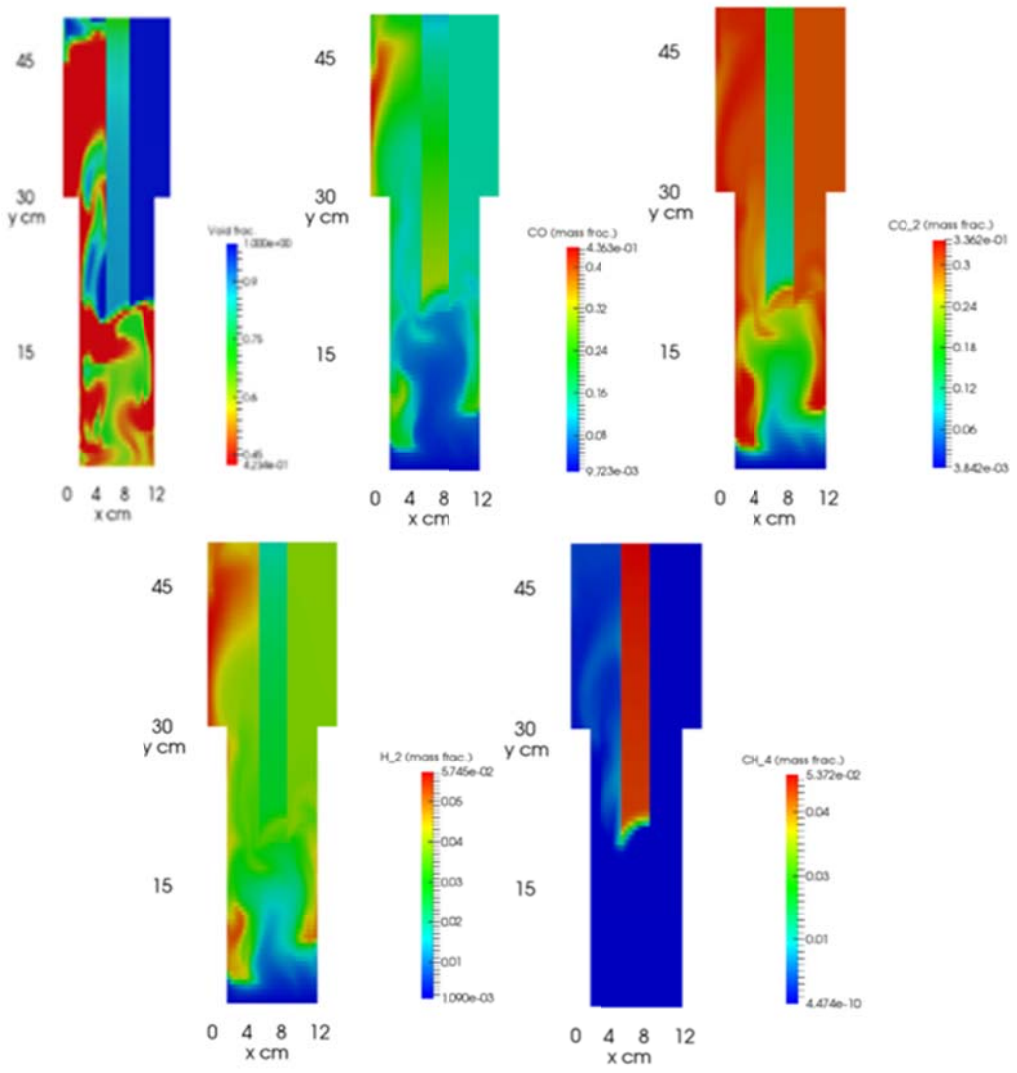

Figure 4.9. Instantaneous distribution of (a) void fraction, (b) CO, (c) CO_2, (d) H_2 and (e) CH_4 concentrations along the reactor at t=260 s.

Figure 4.10 shows comparison of MIX-MCHARS predictions of averaged concentrations with the experimental data [39].To understand the behavior of the mechanism, the kinetics were simplified to a one-dimensional (1D) reactor, similar to that in Ref. [39]. Although all concentration values are approximately consistent with the data, it is evident that CO concentration is underpredicted, while CO_2 is overpredicted. This can be due to disregarding the expansion zone in the 1D case, which leads to higher char concentration at that region. The char fuels the gasification reaction to produce additional CO, which shifts the water-gas shift equilibrium towards more CO_2. Subsequently, we performed the 2D simulations of the fluidized bed. As shown, 2D results show good comparison with the experimental, which is an indication of the accuracy of MFIX-MCHARS.

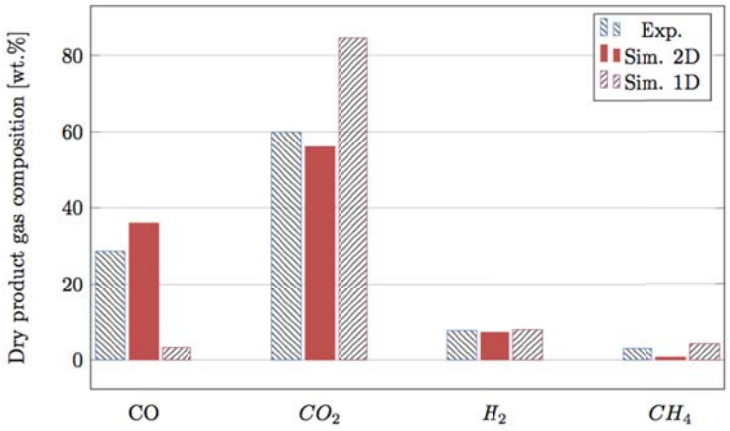

Figure 4.10 – Comparison of MFIX prediction of mean dried gas species concentrations with the experimental data.

5. Computational fluid dynamics simulations (Battaglia)

5.1 Methods

The multifluid Eulerian-Eulerian models employed in the code Multiphase Flow with Interphase eXchanges (MFIX) [38] are used in this work. The instantaneous variables are averaged over a region that is larger than the particle spacing but smaller than the flow domain. Volume fractions are introduced to track the fraction each phase occupies in the averaging volume. The solids phase is described with an effective particle diameter d_p and characteristic material properties, and solved using a conservation equation for the solids phase. The continuity and the momentum equations are solved for both the gas phase and the solids phase and have been presented in [38, 40, 42].

The terms on the left side of the momentum equations include the net rate of momentum increase and the net rate of momentum transfer by convection. The constitutive equations for the gas phase tensor can be found in [38]. The interaction force in the momentum equations accounts for the gas-solids momentum transfer, and the work herein employed the Gidaspow model unless otherwise stated. The granular temperature for the solids phase can be related to the granular energy defined as the specific kinetic energy of the random fluctuating component of the particle velocity.

Kinetic theory for granular flow is used to calculate the solids stress tensor and solid-solids interaction force in the rapid granular flow regime. There are two distinct flow regimes in granular flow: a viscous or rapidly shearing regime in which stresses arise due to collisional or translational momentum transfer, and a plastic or slowly shearing regime in which stresses arise due to Coulomb friction between solids in close contact. A blending function to provide a smooth transition between each regime is employed [38].

The governing equations are discretized using a finite volume approach on a staggered grid to reduce numerical instabilities [46]. Velocities are stored at the cell surfaces, and scalars, such as void fraction and pressure are stored at the center of the cell. Discretization of time derivatives are first order and discretization of spatial derivatives are second-order. An important feature is the use of a second-order discretization scheme for the convective terms, known as the Superbee method, which improves convergence and accuracy of the solution [47]. The SIMPLE algorithm is modified and uses an equation for the solids volume fractions that includes the effect of the solids pressure to help facilitate convergence for both loosely and densely packed regions. A variable time-stepping scheme is also employed to improve convergence and execution speeds.

5.2 Results

5.2.1 Fluidization of coal-biomass mixtures

A thorough understanding of the nature of coal-biomass gasification is not possible without adequate knowledge of the fluidization behavior of the mixture. Therefore in this part of the study, there was considerable focus on fluidization aspects of the co-gasification process. First, the predicted fluidization trends for coal, poplar wood and their binary mixtures were compared with the experiments to determine how the materials behaved. It is important to mention that the particle properties for coal and poplar wood correspond to the Geldart A classification. For both single solids phase of coal and poplar wood, the simulations did not predict the overshoot of pressure drop near U_{mf}, however, the pressure in the unfluidized and fully fluidized regions is predicted accurately for both materials. The dimensionless bed height for both materials also agreed well with experiments. Figure 5.1 shows the pressure drop across the bed and the dimensionless bed height versus gas inlet velocity for the experiments and simulations for coal and poplar wood.

The dimensionless bed height for the three mixtures are presented in Fig. 5.3a-c and show that as the velocity increases, the average bed height expands for each mass ratio. The experiments indicate that as the poplar wood mass ratio increases, the bed height increases. The simulations are in good agreement with the experiments, although a higher bed height is predicted for the 90:10 mass ratio. It is important to note that the 90:10 mass ratio shows similar bed height trends as was seen in the single solids phase for coal fluidization (Fig. 5.1c) with a sudden increase of bed height at medium velocities. As the poplar wood mass ratio increases to 30%, the bed height trends are more similar to the single solids phase of poplar (Fig. 5.1d), where bed height increases more uniformly. The bed height of the 80:20 mass ratio may be interpreted as a transitional state from a bed with properties consistent with coal to a bed with properties more similar to poplar. The sudden increase in bed height at the minimum fluidization velocity is still obvious for the 80:20 mass ratio, although less dramatic than the 90:10 mass ratio. It is also interesting to note that the bed height of the mixtures is higher than the bed height when poplar wood fluidized as a single solids phase but lower than the bed height when coal fluidized as a single solids phase (comparing Figures 5.1 and 5.3).

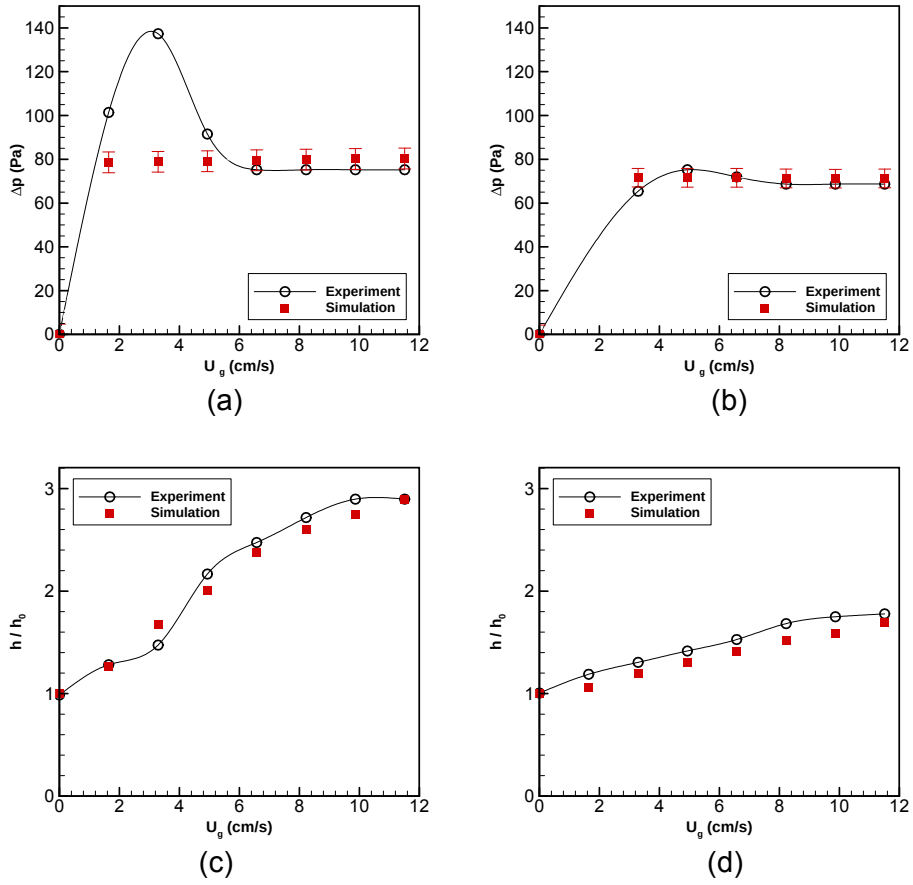

Figure 5.1. Pressure drop versus the gas inlet velocity comparing experiments and simulations for (a) coal, (b) poplar wood, and the dimensionless bed height for different gas inlet velocities comparing experiments and simulations for (a) coal and (b) poplar wood.

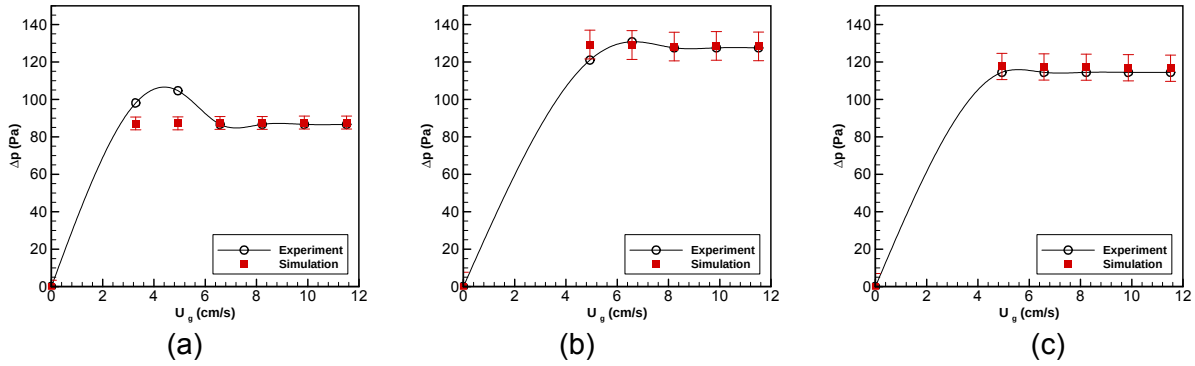

Figure 5.2. Pressure drop versus the gas inlet velocity comparing experiments and simulations for mass ratios for (a) 90:10, (b) 80:20 and (c) 70:30 mass ratio of coal-poplar.

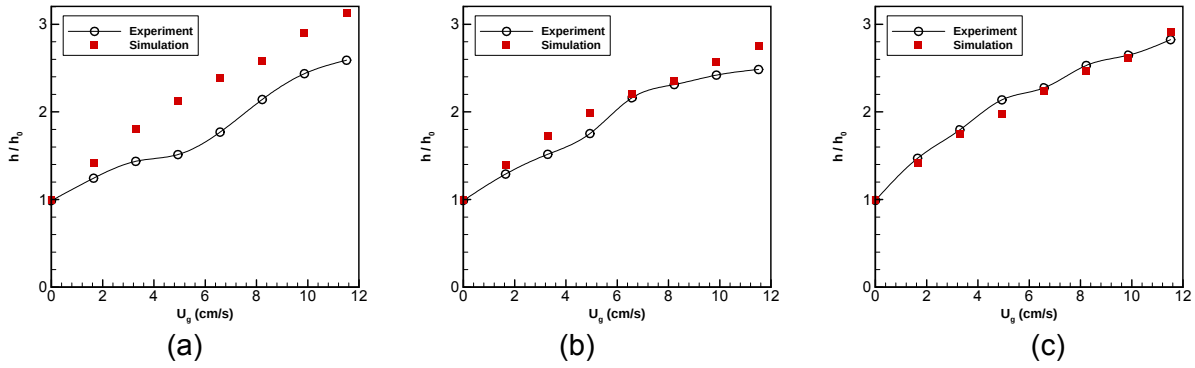

Figure 5.3. The dimensionless bed height for different gas inlet velocities comparing experiments and simulations for mass ratios for (a) 90:10, (b) 80:20 and (c) 70:30 mass ratio of coal-poplar.

5.2.2 Mixing properties of coal-poplar wood mixtures

Mixing characteristics are an important feature that can induce better particle contact, which is essential for increasing the efficiency of the process and providing a relatively uniform temperature throughout the fluidized bed. To quantify the mixing of particles in a fluidized bed, the mixing index (MI) is one method that is used [48]. The mixing index is defined as:

$$MI = \frac{X_U}{X_T} \times 100\%$$

where X_U is the mass fraction of jetsam particles in the upper region of the bed and X_T is the total mass fraction of the jetsam particles in the whole bed. Higher values of *MI* represent better mixing of particles, whereby *MI*= 100% is a perfectly mixed bed and *MI*= 0 is a completely segregated bed. Considering the upper region of the bed begins at h/h_0= 1, the mixing index at U_g = 9.87 cm/s for 90:10, 80:20, and 70:30 mass ratios is 60.69%, 61.92%, and 64.12%, respectively.

The instantaneous gas and solids volume fraction contours for coal and poplar wood at t = 30 s for the three mass ratio mixtures are presented in Fig. 5.4 for U_g = 9.87 cm/s. As the poplar

wood mass ratio increases, void fraction contours (Fig. 5.4a) show a more gas dilute bed, where there are regions of lower void fraction (corresponding to 0.6 that are medium blue) for the 70:30 mass ratio. The size of the bubbles (red regions in all figures) does not show any significant difference between each mass ratio. Instantaneous solids volume fraction contours (Fig. 5.4b-c) show that the regions of higher concentration of coal and poplar wood are mostly coincident, which confirms suitable mixing for each mass ratio.

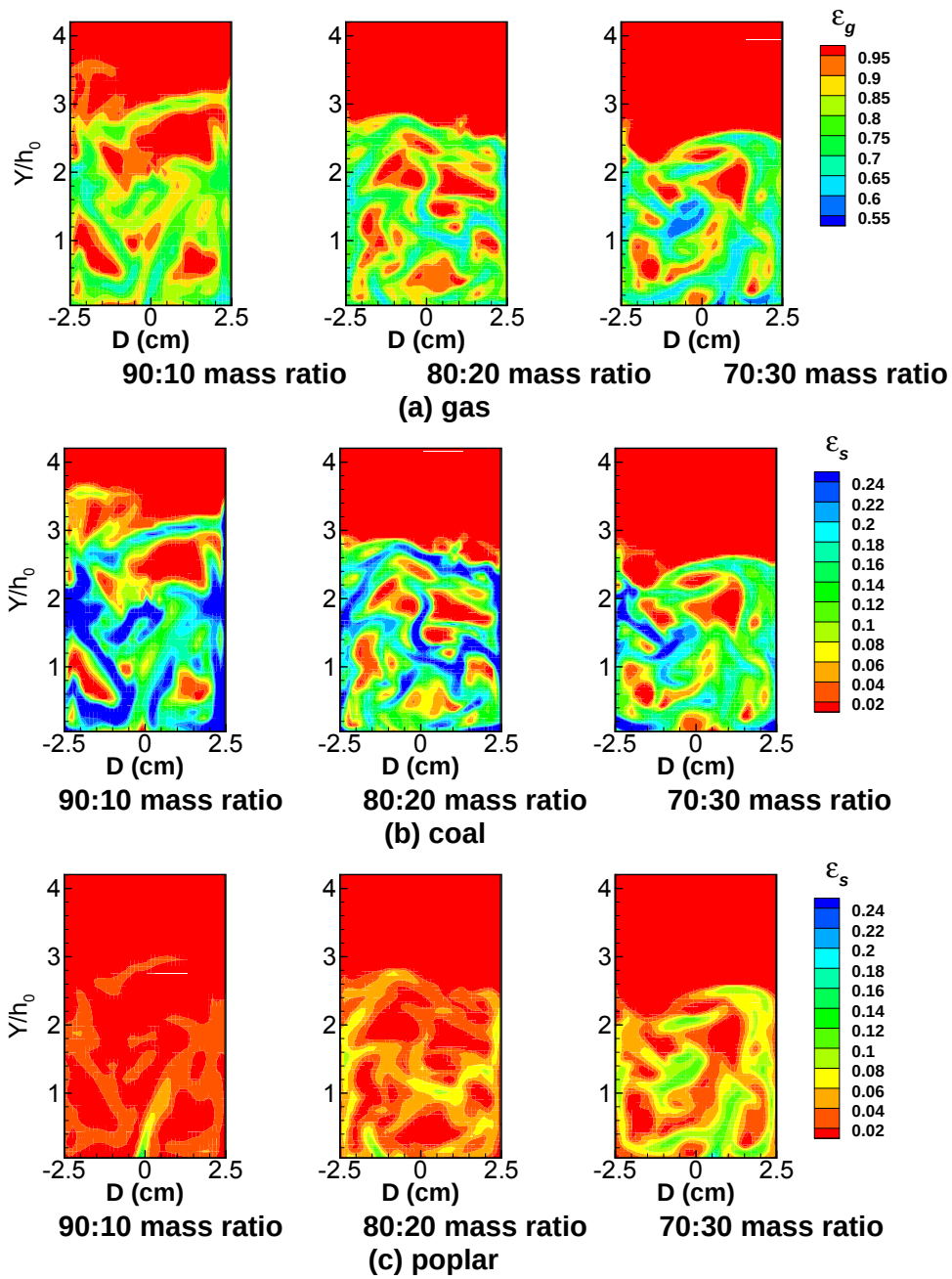

Figure 5.4. Instantaneous volume fraction contours for all mass ratio of coal-poplar using a binary mixture model with U_g = 9.87 cm/s at t =30 s.

5.2.3 Drag models

In order to accurately predict the hydrodynamic behavior of gas and solid phases using an Eulerian-Eulerian approach, it is crucial to use appropriate drag models to capture the correct physics. As a part of this project, the performance of drag models for non-reacting fluidization of Geldart A particles of coal, poplar wood, and their mixtures was assessed. For coal and poplar wood particles, the predicted bed heights using different drag models are presented in Fig. 5.5a-b, respectively, and are compared to the fluidization experiments. For coal, the predicted bed height using each drag model is closer to experiment at lower velocities. However, differences in predicted values become more apparent as inlet gas velocity increases. Based on the predictions for coal, drag models can be roughly divided into two categories: the BVK, HYS, and HKL drag models (group 1) that over-predict bed height, whereas, the Gidaspow, Gidaspow-Blend, Syamlal-O'Brien, and Wen-Yu drag models (group 2) that give good predictions, which are in good agreement with experimental results. For poplar wood, the predicted bed height using all drag models are very similar and agree well with the experiments. It is interesting to note that for poplar wood (Fig. 5b), category 1 predictions are closer to the experiments. However, the trend still persists that category 1 model predictions are still larger than category 2.

The bed height of coal-poplar wood mixtures using different drag models are compared with experimental data, as presented in Fig. 5.6a, b and c for 90:10, 80:20, and 70:30 mass ratios, respectively. Similar to single solid phases, for the 90:10 mass ratio (Fig. 5.6a), the two groups of drag models defined earlier are still recognizable. Similarly, the first group of drag models consisting of BVK, HYS, and HKL drag models over-predicts the bed height whereas the second group of drag models (Gidaspow, Gidaspow-blend, Syamlal-O'Brien, and Wen-Yu) give better predictions that agree well with experiments. Amongst the first group of drag models, the BVK and HKL drag models predict the lowest and highest bed height of the three models, respectively. As poplar wood mass ratio increases, the bed height predicted by the two groups of drag models become more similar, which is similar to the single solids phase of poplar wood (Fig. 5.6b). For mass ratios of 80:20 and 70:30, all drag models except the HKL drag model give good predictions for bed height and agree well with experiments. It is important to mention that for binary mixtures, the HKL drag model always over-predicts the bed height.

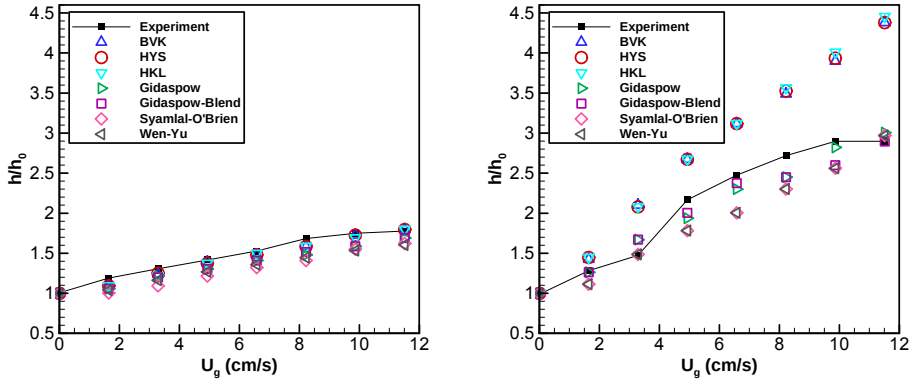

Figure 5.5. Bed height of (a) coal and (b) poplar wood for different drag models compared to experiments.

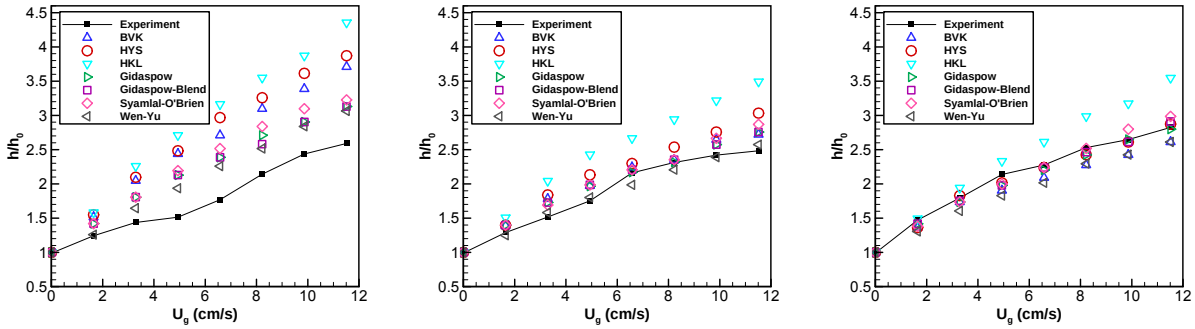

Figure 5.3. Bed height of (a) 90:10, (b) 80:20, and (c) 70:30 coal-poplar wood mass ratio for different drag models compared to experiments.

Overall, the drag models in group 1 predict the fluidization behavior of fine particles of Geldart A more imprecisely. The reason could be due to the numerical nature of the models in category 1. Lattice-Boltzmann simulations were used to calculate the drag force on a system of fixed particles, either arranged in arrays or randomly dispersed. Simulations were repeated for numerous cases to represent a range of Reynolds numbers and solids volume fractions. The calculated drag forces from the Lattice-Boltzmann simulations were then used to create the drag correlations of category 1 and may not be as robust for use in continuum-based Eulerian simulations. In contrast, category 2 drag models were derived from empirical relationships that use void fraction regimes to adjust the formulations, which worked better with Geldart A particles. The HKL model is the only Lattice-Boltzmann model that specifies different formulations based on regimes (using solids volume fraction), however, this model consistently over-predicted bed expansion. Although all drag models of Group 2 are recommended for Geldart A particles when unfluidized regions are not considered in the mass of the bed, for binary mixtures, the Gidaspow-blend and Wen-Yu models performed better than the rest. For single solids phase of coal, for which there were more differences in the predictions, the Gidaspow-blend drag model shows the best performance.

5.3 Gasification Simulations

Simulations were performed to assess and compare the simulations with the gasification experiments conducted in Task 2. Coal was gasified at 700 °C in a nitrogen atmosphere was conducted using the kinetics model provided by Task 3. The fluidization and feed sweep streams were pure N_2 with velocities of 13.2 and 80.7 cm/s respectively, while introducing pulverized coal at a rate of 200 g/hr. The reactions used in the analysis are shown in Table 5.1.

Table 5.1. Simplified reaction model for coal

$$Moisture \rightarrow H_2O \quad (5.1)$$

$$Coal \rightarrow 44.39Char + 0.76CH4 + 1.18CO + 2.53CO_2 + 1.44Tar + 2.09H_2O + 5.57H_2 \quad (5.2)$$

$$Char + H_2O \rightarrow H_2 + CO \quad (5.3)$$

$$Char + CO_2 \rightarrow 2CO \quad (5.4)$$

$$Char + 2H_2 \rightarrow CH_4 \quad (5.5)$$

$$CO + 3H_2 \rightleftarrows CH_4 + H_2O \quad (5.6)$$

$$CO + H_2O \rightleftarrows CO_2 + H_2 \quad (5.7)$$

$$Tar \rightarrow 14.3Char + 0.5CH_4 + 0.7H_2 \quad (5.8)$$

The thermochemical properties of coal, char, and tar were taken from C3M documentation, while their molecular weights were determined via stoichiometry of Eqs. 5.1, 5.3 and 5.8. The instantaneous volume fraction of the gas and both solids phases is shown in Fig. 5.7 with their corresponding phase velocity vectors. Only the lower portion of the domain is shown (below 10 cm). The instantaneous species are shown in Fig. 5.8 to demonstrate where the reactions are occurring (note that the full reactor domain is shown). Table 5.2 shows the effluent gas composition averaged over time and space at the reactor exit.

Table 5.2. Composition of Simulation Effluent Gases

Species	Mass Fraction	Mass Fraction (N_2 free)	Mole Fraction	Mole Fraction (N_2 free)
CO	0.0004	0.0386	0.0004	0.0332
CO_2	0.0013	0.1299	0.0008	0.0712
H_2	0.0001	0.0132	0.0018	0.1574
H_2O	0.0051	0.5052	0.0079	0.6766
CH4	0.0001	0.0145	0.0003	0.0218
TAR	0.0030	0.2987	0.0005	0.0398
N_2	0.9900	----	0.9884	

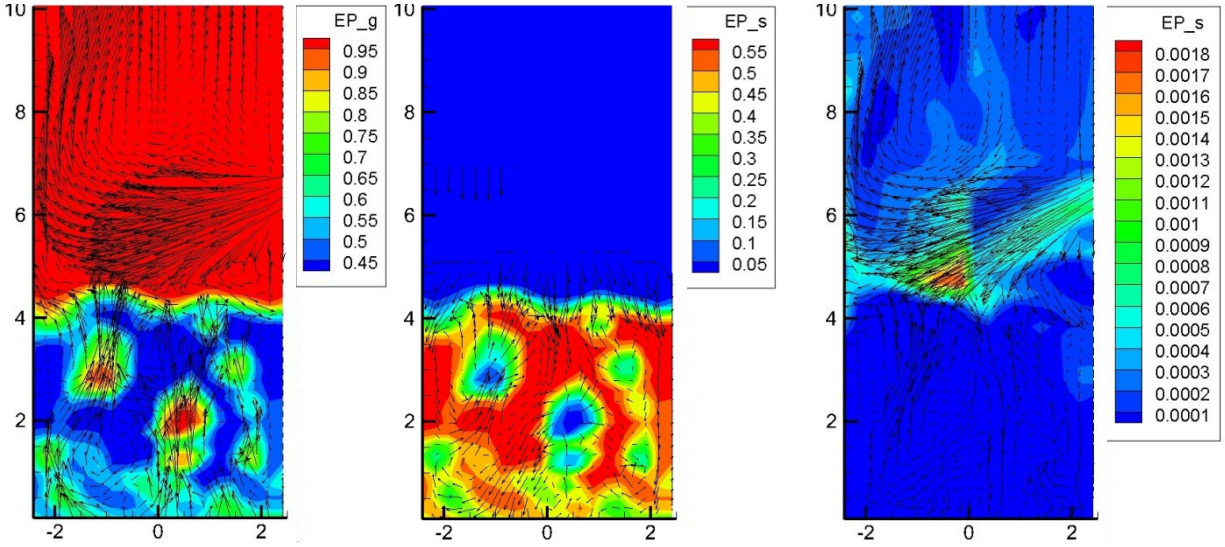

Figure 5.7. Instantaneous (a) gas, (b) sand and (c) coal/char volume fractions superimposed with corresponding velocity vectors.

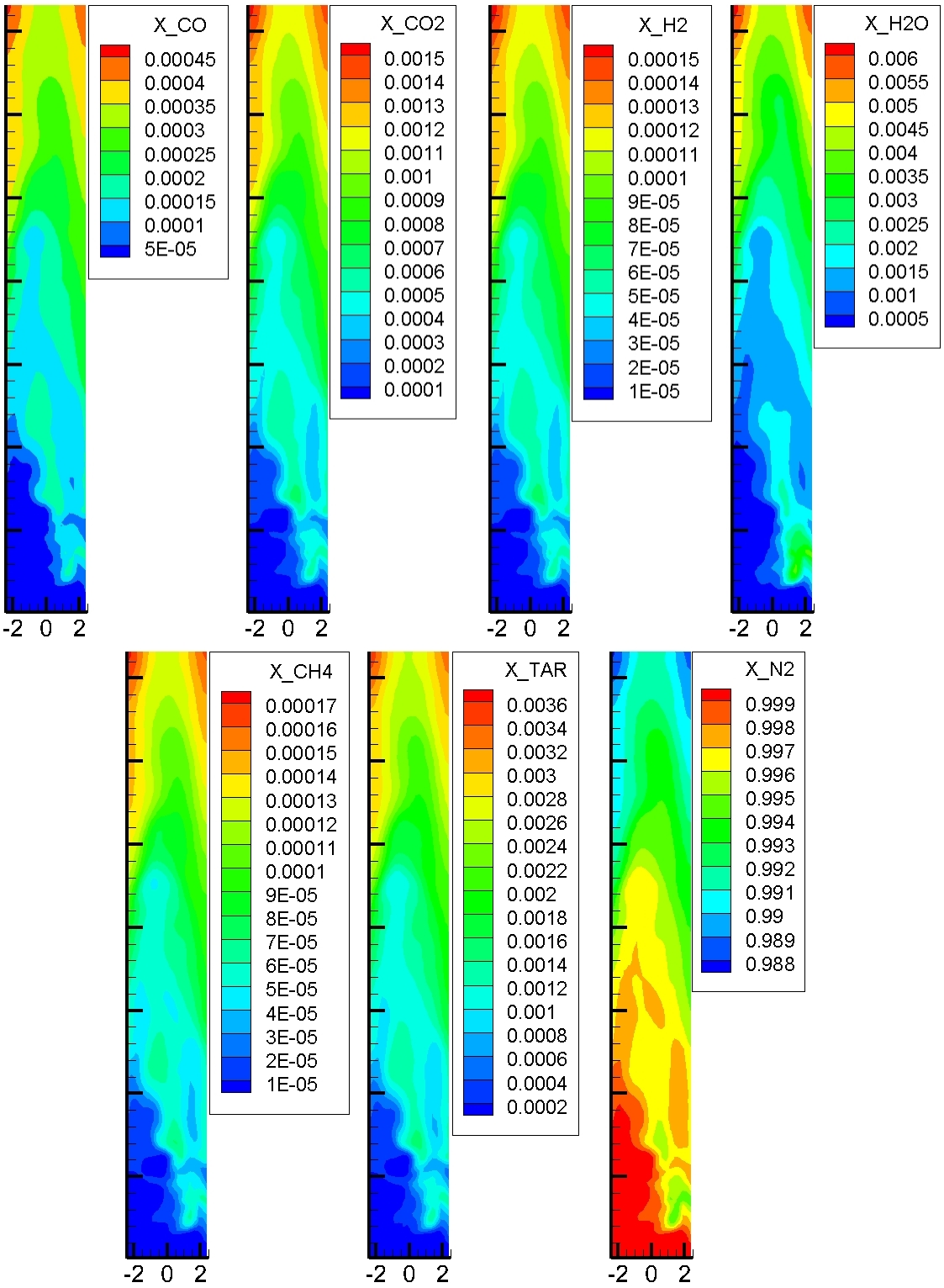

Figure 5.8. Instantaneous gas mass fractions for CO, CO_2, H_2, steam, methane, water, N_2 (left to right, top to bottom).

6. Conclusions

Experiments were conducted to assess the co-gasification of coal and biomass. The biomass materials tested included poplar-wood, corn stover and switchgrass. Red mud was also used as a catalyst and its synergistic effect was examined in the co-gasification studies. Gasification was tested at temperatures of 700, 800 and 900 °C and the ratio of coal to biomass material was increased from 0 to 50% (by weight) in increments of 10 wt.%.

The major gaseous products from co-gasification experiments were H_2, CO, CO_2, and CH_4. Light molecular weight hydrocarbons (C_2-C_4) were present but at very low concentrations. The co-gasification of poplar wood with coal showed similar trends as the corn stover/coal mixtures except that poplar/coal mixtures did not form any agglomerates when silica sand was used in the fluidized bed reactor. The co-gasification behavior of sub-bituminous coal and hybrid poplar wood mixtures using different media (N_2, CO_2) at low temperatures in a fluidized bed showed additive behavior between coal and poplar co-gasification, which indicated lack of synergetic effects. It appeared the two feedstocks underwent thermal degradation independently, which could be attributed to different temperatures of devolatilization for coal and biomass. In spite of lack of major synergies between coal and poplar, co-gasifying the two feedstocks should be considered a key to a sustainable natural resource management since these mixtures did not form any agglomerates.

The red mud appeared to promote cracking of char and tars into product gases as their yields were lower compared to those obtained using silica sand. Product gas yields obtained using red mud were slightly higher than product gas yields from silica sand experiments. This could be due to the catalytic effect of red mud compared to silica sand. In the absence of the biomass in the coal, there was strong water gas shift reaction (Table 15) at 700 ^{o}C which generated a high H2/CO ratio (2.9). Under these conditions, the water gas shift reaction was very vigorous, and therefore most of the CO produced from the coal was consumed in the water gas shift reaction.

Thus, for the red mud reaction, in the case of the pure coal, the H2/CO ratio decreased with temperature whereas in the case of the coal/corn stover mixture, the ratio remained almost constant. This is a very important finding because it shows how the addition of biomass to coal using red mud as a catalyst can alter the H2/CO ratio and therefore the gaseous products can be tailored to various applications such as Fischer Tropsch liquids or use directly as syngas for combustion. Additionally, the red mud was able to reduce tar formation in the product gas. Also of noteworthy was the absence of agglomeration reaction in the reactor. The alkali metals in the corn stover did not form any agglomerates with the red mud which makes the red mud an ideal gasification medium for coal and biomass mixtures.

Over the course of this project, a number of kinetic models were developed for the gasification of coal, and the co-gasification with biomass. These models spanned a large range of detail and utility, and ultimately a few conclusions could be made. For simple lumped models, it is possible to predict the behavior of the biomass fractions. As the detail on the lumps improved, the behavior of the biomass became more unpredictable. A more in depth analysis of the biomass and its tar species would help to alleviate this short coming.

The condensation of the tar back into char is a major source of the solids in the effluent and should not be overlooked in the models. It is possible to model non-oxygen based gasification without considering the diffusion or any type of shrinking core (reactions occur slower as gasification conversion proceeds) or random pore model (reactions occur faster as gasification conversion proceeds). The complexity of a fully molecular model of gasification technology is governed not by the gasification reactions, but by the pyrolysis and the overabundance of tar species.

Attribute reaction modeling may be possible with a much more in depth analysis of the feed solids and the effluent solids and tars. If we put wet coal and gas into the gasifier, there is

enough water produced from drying to drive the steam gasification reactions. It is important to understand the abilities and shortcomings of modeling the kinetics and the computational fluid dynamics so as to produce the proper interface between the two modeling technologies. Future efforts should be able to capitalize on the structure of the tuned models, and with a number of different models available, choose one appropriate for the work at hand. Finally, we have shown the optimal framework for linking kinetic behavior with fluid dynamic design.

Simulations were performed using MFIX and coupled with a newly designed reaction module to facilitate handing of complex chemical kinetics, MCHARS. The interface improved the efficiency of multi-phase reacting flow calculations by splitting the hydrodynamics and chemistry calculation into separate fractional steps. This splitting also improved flexibility and computational efficiency of both solvers.

An important issue is the role that numerics plays in reliable prediction of bubble dynamics and hence, mixing and chemical reaction in the bed. Simulations were performed using first order upwind, and higher order TVD schemes such as Superbee and Monotonized Central, together with deferred correction and downwind weighting factor methods. The TVD schemes gave good prediction of bubble and particle dynamics; whereas, excessive numerical diffusion in upwind cause unrealistic behavior of the flow. Among the TVD schemes, MC provides favorable prediction of fluidization with relatively less computational cost. Also, the DWF algorithm was computationally advantageous due to its parallel efficiency on distributed memory platforms.

Numerical simulations of fluidized beds were used to better understand the fluidization and particle mixing behavior of coal-biomass mixtures. Also simulations were used to find the best drag model between seven models reported in the literature to simulate coal, poplar wood, and their mixtures. The predictions for pressure drop across the bed and bed height were validated with the experiments and found to be in a good agreement. Pressure drop for the coal-poplar mixtures were higher than single solids phases for each material, however, the pressure of the 90:10 mass ratio was close to the single solids phase pressure drop. It was found that the 90:10 mass ratio exhibited bed height trends similar with the single solids phase of coal, and as the poplar wood mass ratio increased to 30%, the bed height trend was similar to the single solids phase of poplar wood. Although instantaneous solid volume fraction contours indicated good mixing characteristics for all mass ratio mixtures, solids mass flux and velocity vectors showed a tendency of better mixing for mixtures with higher poplar mass ratio. A quantitative analysis of the mixing index confirmed that as the poplar wood mass ratio increased, the quality of mixing improved, with an average mixing index of 62%. Therefore, reasonable amounts of biomass can be added with coal without adverse effects of segregation or elutriation, while reducing the use of a fossil fuel.

Results of the drag model study revealed that if static regions of material are removed by adjusting the mass in the fluidized bed, the commonly-used drag models for Geldart B particles work well with Geldart A particles. The Gidaspow-blend model proved to be the more reliable drag model for both single solid phases and binary mixtures. These conclusions were also substantiated by examining void fraction profiles to demonstrate particle distribution. Studying the nature of the two groups of models revealed that the first group used numerical simulations to derive drag force models, whereas the second group models were derived from empirical correlations. These models were coupled with the kinetics modeling using a simplified set of reactions for the gasification simulations. The experimental data was used to validate the simulations and overall the results indicated that the simplified model provided good predictions of the gasification.

The gas-solid reacting flow simulations were carried out using MFIX coupled with our new reaction module. This module provides an efficient and convenient means to implement reactions in MFIX. The gain in computational efficiency is because the reaction module uses the

fractional steps method, which is proven useful by separating integration of the chemical reaction into fractional steps. Using this approach the transport equations are advanced with the flow time scale and the integration of chemical reaction is handled using a standard stiff ordinary differential equation solver. This effort includes extensive assessment of the module against the results obtained using original MFIX and validations against experimental data. The former shows almost identical comparison between reaction module and original MFIX results. Coal kinetics has been implemented in the module and simulations were performed using MFIX-MCHARS. Predictions showed favorable agreement with the experimental data. This study demonstrated the capacity of the reaction module to handle chemical mechanisms as well as its accuracy and efficiency in gas-solid reacting flow simulations. This module can be used in the future to consider reaction mechanisms with various levels of complexity in MFIX simulations.

References

[1] Peng, Y., and Fan, L. T., 1995, "Hysteresis in liquid-solid tapered fluidized beds," Chemical Engineering Science, 50(16), pp. 2669-2671.

[2] Heck, J., and Onken, U., 1987, "Hysteresis effects in suspended solid particles in bubble columns with and without draft tube," Chemical Engineering Science, 42(5), pp. 1211-1212.

[3] Jackson, R., 1998, "The nature and role of effective stress in fluidized systems," 9th Fluidization - Engineering Foundation Conference, Engineering Foundation, New York, pp. 1-14.

[4] Loezos, P. N., Costamagna, P., and Sundaresan, S., 2002, "The role of contact stresses and wall friction on fluidization," Chemical Engineering Science, 57(24), pp. 5123-5141.

[5] Srivastava, A., and Sundaresan, S., 2002, "Role of wall friction in fluidization and standpipe flow," Powder Technology, 124(1–2), pp. 45-54.

[6] Tsinontides, S., and Jackson, R., 1993, "The mechanics of gas fluidized beds with an interval of stable fluidization," Journal of Fluid Mechanics, 255, pp. 237-274.

[7] Weber, M. W., and Hrenya, C. M., 2007, "Computational study of pressure-drop hysteresis in fluidized beds," Powder Technology, 177(3), pp. 170-184.

[8] Pattipati, R. R., and Wen, C., 1981, "Minimum fluidization velocity at high temperatures," Industrial & Engineering Chemistry Process Design and Development, 20(4), pp. 705-707.

[9] Reina, J., Velo, E., and Puigjaner, L., 2000, "Predicting the minimum fluidization velocity of polydisperse mixtures of scrap-wood particles," Powder Technology, 111(3), pp. 245-251.

[10] Formisani, B., Girimonte, R., and Longo, T., 2008, "The fluidization process of binary mixtures of solids: Development of the approach based on the fluidization velocity interval," Powder Technology, 185(2), pp. 97-108.

[11] Lin, C.-L., and Wey, M.-Y., 2004, "The effect of mineral compositions of waste and operating conditions on particle agglomeration/defluidization during incineration," Fuel, 83(17), pp. 2335-2343.

[12] Parveen, F., Berruti, F., Briens, C., and McMillan, J., 2013, "Effect of fluidized bed particle properties and agglomerate shape on the stability of agglomerates in a fluidized bed," Powder Technology, 237, pp. 46-52.

[13] Basu, P., and Sarka, A., 1983, "Agglomeration of coal ash in fluidized beds," Fuel, 62(8), pp. 924-926.

[14] Bell, D. A., Towler, B. F., and Fan, M., 2010, Coal gasification and its applications, William Andrew.

[15] Lin, W., Dam-Johansen, K., and Frandsen, F., 2003, "Agglomeration in bio-fuel fired fluidized bed combustors," Chemical Engineering Journal, 96(1), pp. 171-185.

[16] Fryda, L., Panopoulos, K., and Kakaras, E., 2008, "Agglomeration in fluidised bed gasification of biomass," Powder technology, 181(3), pp. 307-320.

[17] Zhang, L., Xu, S., Zhao, W., and Liu, S., 2007, "Co-pyrolysis of biomass and coal in a free fall reactor," Fuel, 86(3), pp. 353-359.

[18] Gao, C., Vejahati, F., Katalambula, H., and Gupta, R., 2009, "Co-gasification of biomass with coal and oil sand coke in a drop tube furnace†," Energy & Fuels, 24(1), pp. 232-240.

[19] Hernández, J. J., Aranda-Almansa, G., and Serrano, C., 2010, "Co-gasification of biomass wastes and coal− coke blends in an entrained flow gasifier: an experimental study," Energy & Fuels, 24(4), pp. 2479-2488.

[20] Krerkkaiwan, S., Fushimi, C., Tsutsumi, A., and Kuchonthara, P., 2013, "Synergetic effect during co-pyrolysis/gasification of biomass and sub-bituminous coal," Fuel Processing Technology, 115, pp. 11-18.

[21] Collot, A. G., Zhuo, Y., Dugwell, D. R., and Kandiyoti, R., 1999, "Co-pyrolysis and co-gasification of coal and biomass in bench-scale fixed-bed and fluidised bed reactors," Fuel, 78(6), pp. 667-679.

[22] Zhu, W., Song, W., and Lin, W., 2008, "Catalytic gasification of char from co-pyrolysis of coal and biomass," Fuel Processing Technology, 89(9), pp. 890-896.

[23] Idris, S. S., Rahman, N. A., Ismail, K., Alias, A. B., Rashid, Z. A., and Aris, M. J., 2010, "Investigation on thermochemical behaviour of low rank Malaysian coal, oil palm biomass and their blends during pyrolysis via thermogravimetric analysis (TGA)," Bioresource technology, 101(12), pp. 4584-4592.

[24] Brar, J., Singh, K., Wang, J., and Kumar, S., 2012, "Cogasification of coal and biomass: a review," International Journal of Forestry Research, 2012.

[25] Kumabe, K., Hanaoka, T., Fujimoto, S., Minowa, T., and Sakanishi, K., 2007, "Co-gasification of woody biomass and coal with air and steam," Fuel, 86(5), pp. 684-689.

[26] Collot, A.-G., Zhuo, Y., Dugwell, D., and Kandiyoti, R., 1999, "Co-pyrolysis and co-gasification of coal and biomass in bench-scale fixed-bed and fluidised bed reactors," Fuel, 78(6), pp. 667-679.

[27] Li, K., Zhang, R., and Bi, J., 2010, "Experimental study on syngas production by co-gasification of coal and biomass in a fluidized bed," International journal of hydrogen energy, 35(7), pp. 2722-2726.

[28] Basu, P., 2010, Biomass gasification and pyrolysis: practical design and theory, Academic press.

[29] Rajvanshi, A. K., 1986, "Biomass gasification," Alternative energy in agriculture, 2(4), pp. 82-102.

[30] Wiser, W., 1973, "Proceedings of the Electric Power Research Institute Conference on Coal Catalysis," Santa Monica, CA, pp. 3-62.

[31] Everson, R. C., Neomagus, H. W., Kasaini, H., and Njapha, D., 2006, "Reaction kinetics of pulverized coal-chars derived from inertinite-rich coal discards: gasification with carbon dioxide and steam," Fuel, 85(7), pp. 1076-1082.

[32] Williams, A., Backreedy, R., Habib, R., Jones, J. M., and Pourkashanian, M., 2002, "Modelling coal combustion: the current position," Fuel, 81(5), pp. 605-618.

[33] Roberts, M. J., Everson, R. C., Domazetis, G., Neomagus, H. W., Jones, J., Van Sittert, C. G., Okolo, G. N., Van Niekerk, D., and Mathews, J. P., 2015, "Density functional theory molecular modelling and experimental particle kinetics for CO 2–char gasification," Carbon, 93, pp. 295-314.

[34] Horton, S. R., Hou, Z., Moreno, B. M., Bennett, C. A., and Klein, M. T., 2013, "Molecule-based modeling of heavy oil," Science China Chemistry, 56(7), pp. 840-847.

[35] Xu, J., and Qiao, L., 2012, "Mathematical modeling of coal gasification processes in a well-stirred reactor: effects of devolatilization and moisture content," Energy & Fuels, 26(9), pp. 5759-5768.

[36] Bradley, D., Lawes, M., Park, H.-Y., and Usta, N., 2006, "Modeling of laminar pulverized coal flames with speciated devolatilization and comparisons with experiments," Combustion and flame, 144(1), pp. 190-204.

[37] Merrick, D., 1983, "Mathematical models of the thermal decomposition of coal: 1. The evolution of volatile matter," Fuel, 62(5), pp. 534-539.

[38] Syamlal, M., Rogers, W., and O'Brien, T. J., 1993, "MFIX documentation: Theory guide," National Energy Technology Laboratory, Department of Energy, Technical Note DOE/METC-95/1013 and NTIS/DE95000031.

[39] Gidaspow, D., 1994, Multiphase flow and fluidization: continuum and kinetic theory descriptions, Academic press.

[40] Deza, M., Franka, N. P., Heindel, T. J., and Battaglia, F., 2009, "CFD Modeling and X-Ray Imaging of Biomass in a Fluidized Bed," ASME Journal of Fluids Engineering, 131(11).

[41] Guenther, C., and Syamlal, M., 2001, "The effect of numerical diffusion on simulation of isolated bubbles in a gas–solid fluidized bed," Powder Technology, 116(2–3), pp. 142-154.

[42] Xie, N., Battaglia, F., and Pannala, S., 2008, "Effects of using two- versus three-dimensional computational modeling of fluidized beds - Part I, hydrodynamics," Powder Technology, 182(1), pp. 1-13.

[43] Xie, N., Battaglia, F., and Pannala, S., 2008, "Effects of using two- versus three-dimensional computational modeling of fluidized beds: Part II, budget analysis," Powder Technology, 182(1), pp. 14-24.

[44] Xie, N., Battaglia, F., and Fox, R. O., 2004, "Simulations of multiphase reactive flows in fluidized beds using in situ adaptive tabulation," Combustion Theory and Modelling, 8(2), pp. 195-209.

[45] Neogi, D., 1984, "Coal Gasification in an Experimental Fluidized-Bed Reactor,"M.S., Kansas State University.

[46] Syamlal, M., 1998, "MFIX documentation: Numerical technique," National Energy Technology Laboratory, Department of Energy, Technical Note No. DOE/MC31346-5824.

[47] Syamlal, M., 1997, "Higher order discretization methods for the numerical simulation of fluidized beds," EG and G Technical Services of West Virginia, Inc., Morgantown, WV (United States).

[48] Rowe, P. N., and Nienow, A. W., and Agbim, A. J., 1972, "A Preliminary Quantitative Study of Particle Segregation in Gas Fluidised Beds - Binary Systems of Near Spherical Particles," Transactions of the Institution of Chemical Engineers, 50, p. 310.